


6-30-2010

Gold Nanoparticles and Their Polymer Composites: Synthesis Characterization and Applications

Nidhi Joshi

University of South Florida

Follow this and additional works at: <https://digitalcommons.usf.edu/etd>

 Part of the [American Studies Commons](#), and the [Mechanical Engineering Commons](#)

Scholar Commons Citation

Joshi, Nidhi, "Gold Nanoparticles and Their Polymer Composites: Synthesis Characterization and Applications" (2010). *Graduate Theses and Dissertations*.
<https://digitalcommons.usf.edu/etd/3516>

This Thesis is brought to you for free and open access by the Graduate School at Digital Commons @ University of South Florida. It has been accepted for inclusion in Graduate Theses and Dissertations by an authorized administrator of Digital Commons @ University of South Florida. For more information, please contact scholarcommons@usf.edu.

Gold Nanoparticles and Their Polymer Composites: Synthesis Characterization and
Applications

by

Nidhi Joshi

A thesis submitted in partial fulfillment
of the requirements for the degree of
Master of Science
Department of Mechanical Engineering
College of Engineering
University of South Florida

Major Professor: Ashok Kumar, Ph.D.
John Wolan, Ph.D.
Garrett Matthews, Ph.D.

Date of Approval:
June 30, 2010

Keywords: Nanotechnology, Surface Plasmon Resonance, Biosensors, RSV, Catalyst

Copyright © 2010, Nidhi Joshi

Dedication

My son Manas. You are my life

My husband Rakesh. For always being there for me and supporting me throughout.

Acknowledgments

I feel very fortunate to have had Professor Ashok Kumar as my thesis supervisor. He introduced me to this fascinating area of nanoparticle research. His guidance, support and encouragement through the course of my research have made it one of my most treasured experiences. I would also like to thank my committee members Dr. Johan Wolan and Dr. Garrett Mathews for their invaluable suggestions and support.

I want to thank Dr. Subbiah Alwarappan and Dr. M. K. Ram for their help in electrochemistry related experiments. My sincere thanks are due to Dr. Yusuf for TEM experiments. I also thank Mr. Sung for help related to SERS experiments. I want to thank Seyhan and Dr. Shree Ram Singh for RSV related experiments.

Words fail to express my gratitude towards my Parents for teaching me that hard work is the only key to success. I cannot forget to thank Somu and Ashu for their love and support. I greatly acknowledge the moral support and strength I received from my parent's in-laws and family members. I am indebted to my father in law Dr. T. D. Joshi for encouraging me to build my career in the field of research.

I offer my regards to all my lab mates and friends who supported me in any respect during the completion of the project. My special thanks are due to Supriya and Makhan.

This work is financially supported by the national science foundation grant CREST#0734232

Table of Contents

List of Tables	iii
List of Figures	iv
Abstract	vii
Chapter 1: Introduction	1
1.1 Metal Nanoparticles	1
1.2 Gold Nanoparticles	1
1.3 Optical Properties of Gold Nanoparticles	3
1.3.1 Surface Plasmon Resonance	3
1.4 Composites of Polymer-Gold Nanoparticles	6
Chapter 2: Experimental Methods	8
2.1 Introduction	8
2.2 Materials	8
2.3 Synthesis of Gold Nanoparticles (GNPs)	8
2.3.1 Citrate Reduction Method	8
2.3.2 Bio-Compatible Gold Nanoparticles	9
2.3.3 Synthesis of GNPs Stabilized with Poly Vinyl Pyrrolidone	9
2.4 Synthesis of Composites of Polymer-Gold Nanoparticles	10
2.5 Characterization Techniques	11
2.5.1 UV-vis Spectrophotometer	11
2.5.2 Transmission Electron Microscopy	13
2.5.3 Fourier Transform Infrared Spectroscopy	15
2.5.4 Atomic Force Microscopy	16
2.5.5 Surface Enhanced Raman Spectroscopy	19
2.5.6 Electrochemical Voltammetry	19
2.5.6.1 Cyclic Voltammetry	20
Chapter 3: Structural and Optical Properties of Gold Nanoparticles	25
3.1 Introduction	25
3.2 Characterization of Au Nanoparticles	25

3.2.1. Absorption Spectroscopy	25
3.2.2 Morphology Analysis of GNPs (TEM).....	30
3.2.3 SERS	36
3.2.4 Atomic Force Microscopy	39
3.2.5 Electrochemical Characterization of GNPs	40
3.3 Characterization of Gold-Polymer Composites	41
3.4 Electrochemical Characterization of GNPs-POAS.....	45
Chapter 4: Applications of GNPs	49
4.1 Introduction.....	49
4.2 RSV Inhibition by GNPs	49
4.2.1 Cells and Virus.....	49
4.2.2 Preparation of GNPs and RSV Mixture.....	50
4.2.3 RSV Inhibition Experiment	50
4.3 Biosensing Applications of the GNPs.....	54
4.3.1 Detection of Neurotransmitters such as Dopamine, Ascorbic Acid.....	55
4.3.1.1 Importance of Monitoring Neurotransmitters.....	56
4.4 Analysis of GNPs-BSA Pair	60
4.5 Catalytic Application of Chemically Synthesized GNPs.....	64
4.5.1 Au Decoration on ZnO Nanowires	64
Chapter 5: Conclusions.....	70
Chapter 6: Future Work	72
References.....	73
About the Author	End Page

List of Tables

Table 3.1 Gold Nanoparticles: Synthetic and Characterizing Parameters.....	36
--	----

List of Figures

Figure 1.1 Surface Plasmon Resonance of Metal Nanoparticles	4
Figure 1.2 Schematic of the Overlapping of Energy Bands in Metal	5
Figure 1.3 Schematic Representations of POAS in Emeraldine Base	7
Figure 2.1 Schematic of the Chemical Assembly for Nanoparticles Synthesis.....	10
Figure 2.2 Schematic of the Oxidative Polymerization	11
Figure 2.3 UV-vis Spectrophotometer Set Up in USF	13
Figure 2.4 Optical Components in TEM.....	14
Figure 2.5 Schematic of Transmission Electron Microscopy in USF	15
Figure 2.6 FTIR.	16
Figure 2.7 Schematic of the Modes of Operation in AFM	18
Figure 2.8 Schematic of Sample Geometry for Nanoparticle Based SERS	19
Figure 2.9 Typical Triangular Wave Form Applied to the Working Electrode.....	21
Figure 2.10 A Typical Cyclic Voltammogram of One Electron Transfer	23
Figure 2.11 Typical Cyclic Voltammogram of Two Electron Transfer	24
Figure 3.1 Absorption Spectrum of the Gold Nanoparticles	26
Figure 3.2 UV-Visible Absorption Spectrum of the Gold Nanoparticles Synthesized by Citrate Reduction Method	27
Figure 3.3 Images of Gold Nanoparticle Solutions	28
Figure 3.4 Absorption Spectra of Gold Nanoparticles (~527 nm, 550 nm and 574 nm.).....	29

Figure 3.5 UV-vis Spectra of Bio-Compatible Gold Nanoparticles	30
Figure 3.6 TEM Images of the Gold Nanoparticles (Boot Shaped)	31
Figure 3.7 TEM Images of GNPs (~5 nm-7 nm).....	32
Figure 3.8 TEM Images of GNPs (~10 nm)	32
Figure 3.9 TEM Images of GNPs (~20 nm)	33
Figure 3.10 TEM Images of GNPs (~20 nm-30 nm).....	33
Figure 3.11 TEM Images of GNPs Nanocubes (~200 nm)	34
Figure 3.12 TEM Images of GNPs (Nanotriangles, Octagons~50 nm-60 nm)	34
Figure 3.13 TEM Images of GNPs (Cubes, Pentagon ~ 100 nm)	35
Figure 3.14 TEM Image GNPs (~10 nm-20 nm).....	35
Figure 3.15 SERS of 5 nm Gold Nanoparticles	37
Figure 3.16 SERS of 10 nm Gold Nanoparticles	38
Figure 3.17 AFM Images of Gold Nanoparticles	39
Figure 3.18 C.V of GNPs 20 nm.E V vs. Ag AgCl in $[\text{Ru}(\text{NH}_3)_6]^{3+/2+}$	41
Figure 3.19 C.V of GNPs 20 nm.E V vs. Ag AgCl in $[\text{K}_4\text{Fe}(\text{CN})_6]^{3-/4-}$	41
Figure 3.20 UV-vis Spectra of POAS.....	42
Figure 3.21 UV-vis Spectra of Composites POAS- GNPs	43
Figure 3.22 TEM Images, (a) POAS, (b) POAS-GNPs.....	44
Figure 3.23 FTIR of (a) GNPs, (b) POAS, (c) POAS-GNPs.....	45
Figure 3.24 CV of POAS in Three Electrode System in 0.1M HCL.....	46
Figure 3.25 CV of POAS -GNPs in Three Electrode System in 0.1M HCL.....	47
Figure 4.1 Schematic of RSV Inhibition Experiment.....	51
Figure 4.2 RSV Inhibition by Immunofluorescence Cells Infected with RSV.....	52

Figure 4.3 Cells Infected with RSV Mixed GNPs (5 μ l/ml)	52
Figure 4.4 Cells Infected with RSV Mixed with GNPs (50 μ l/ml)	53
Figure 4.5 Cells Infected with RSV Mixed with GNPs (100 μ l/ml)	53
Figure 4.6 Cells Infected with RSV Mixed with GNPs (200 μ l/ml)	54
Figure 4.7 Structures of Dopamine and Ascorbic Acid	55
Figure 4.8 Cyclic Voltammogram of Dopamine in PBS	58
Figure 4.9 Scan Rate/Current Density Plot of Dopamine.....	59
Figure 4.10 Cyclic Voltammogram of Ascorbic Acid in PBS.....	60
Figure 4.11 UV-vis Spectra of GNPs and GNPs-BSA (1~10 nm), (2~30 nm)	61
Figure 4.12 (a) TEM of GNPs (~10 nm)	62
Figure 4.12 (b) TEM of GNPs –BSA Complex (GNPs~10 nm)	62
Figure 4.13 (a) TEM of GNPs (~35-40 nm).....	63
Figure 4.13 (b) TEM of GNPs-BSA (~35- 40 nm).....	63
Figure 4.14 (a) TEM Image of GNPs, (b) SEM of ZnO Nanowire-GNPs	65
Figure 4.15 Assemblies of CO Sensors	67
Figure 4.16 Variation of Gas Sensor Signal with CO Gas Concentration for ZnO and Au -ZnO Nanowires at (a) Room Temperature and (b) 200 $^{\circ}$ C	68

Gold Nanoparticles and Their Polymer Composites: Synthesis, Characterization and Applications

Nidhi Joshi

Abstract

Gold nanoparticles are excellent candidates for all the biomedical applications due to their size and shape dependent optical and physiological properties. In this study, gold nanoparticles were synthesized chemically for bio-application. It was observed that the size and shape of gold nanoparticles depend strongly on the concentration of chemical solution, type of reducing agent used in the reaction, temperature of the solution and stabilizing agent for reaction. Transmission electron microscopy (TEM) has been used extensively to determine the size and shape of the gold nanoparticles. Optical properties of the size and shape selected nanoparticles were studied using UV-vis spectrophotometer in absorption mode. The chemically synthesized gold nanoparticles were observed to show excellent absorption property which is reflected by the presence of the characteristic surface plasmon resonance (SPR) band peak. The SPR peak was found to be predominantly dependent on the size of nanoparticles. We have observed a strong red shift with increasing the size of gold nanoparticles. The position of the SPR peak was also observed to change with shape of gold nanostructures.

Synthesis and characterization of the composites of gold nanoparticles and Poly (O-anisidine) (POAS) have been carried out in this thesis. Gold-POAS materials system was

characterized using UV-vis spectroscopy, TEM, Fourier Transform Infrared Spectroscopy.

The chemically synthesized gold nanoparticles were successfully utilized for the study of Respiratory Syncycial Virus (RSV) interaction. Gold nanoparticles were found to inhibit the RSV infection. The electrochemical behavior of gold nanoparticles was studied and their potentials for biosensing applications were tested. Cyclic voltaammetry was performed for the detection of dopamine and ascorbic acid using gold nanoparticles of different sizes. Interaction of gold nanoparticles with Bovine Serum Albumin (BSA) has been studied via absorption spectroscopy and TEM measurements. The absorption spectra of the GNP-BSA show remarkable shift in SPR band peak towards high wavelength. Catalytic properties of the gold nanoparticles were studied by using them as a catalytic activator for the gas sensing applications.

Chapter 1: Introduction

1.1 Metal Nanoparticles

Materials such as multifunctional supermolecules, carbon nanotubes, graphene, and metal nanoparticles have been synthesized and employed routinely as basic building block for several electronic and optical devices. Integration of nanoscale building blocks such as nanoparticles, nanorods and nanotubes into functional assemblies and further into multifunctional devices can be achieved *via* nanotechnology for several applications. Further, the properties of nanomaterials depend on its shape and size. In particular, metal nanoparticles are very interesting nanoscale materials with an ease of synthesis and modification. The advantages of metal nanoparticles over other material include its strong optical and electronic properties [1-7]. The dimensions of the nanoparticles vary between 1 nm to 100 nm and these nanoparticles behave like a whole unit in terms of their properties and transport phenomenon. Furthermore, the properties of nanoparticles are very different than the bulk materials, thereby; nanoparticles are suitable candidates for various biomedical applications.

1.2 Gold Nanoparticles

Of the various metal nanoparticles reported in the literature [1-7], gold is the promising candidate due to its excellent surface properties that can be exploited in biotechnological,

optical and electrochemical applications. The advantages of the gold nanoparticles include non-toxicity, strong scattering length, bio-conjugation and long-term stability. These characteristics are essential for a stable and sensitive biosensing platform. Gold nanoparticles offer excellent optical properties and exhibit a spectral shift upon varying their size and shape. Gold nanoparticles exhibit a characteristic absorption peak at 525 nm and this peak will shift towards the higher wavelength region by tuning the size and shape of the nanoparticles. Optical properties of the Au nanoparticles can be varied by controlling their size and also by modifying their surface characteristics. The size and the surface characteristics are related to the surface to volume ratio.

The electron transfer or the conductive behavior of the metal nanoparticles has been studied recently within the context of reduced electronic device size features to the nanoscale level. Unlike bulk materials, the conductivity is not based on the band structure but shows single electron tunneling through discrete energy level. Gold is often considered as a suitable material for electronic devices, because, gold nanoparticles can be synthesized with diameters ranging between 2 nm and 100 nm. On the other hand, the highly reactive surface of the gold can be very easily modified with polymers, silicates and biomolecules. As a result, gold nanoparticles are widely employed as a platform to design a stable and sensitive biosensor.

In this work, we have synthesized gold nanoparticles of various size and shape by different techniques such as sodium citrate reduction method, anisotropic synthesis by using PVP and biocompatible gold nanoparticles. Following this, we have then evaluated the interaction of gold nanoparticles with biomolecules

1.3 Optical Properties of Gold Nanoparticles

1.3.1 Surface Plasmon Resonance

Surface Plasmon Resonance (SPR) is an optical phenomenon caused by the interaction of the surface Plasmon with the incident electromagnetic radiation at a resonant frequency. Metals exhibit plasmon effect because they have a high density of free electrons. The sensitivity of the plasmon depends on particle size, shape, the refractive index of the medium and the dielectric constants of the metal. For several metals the plasmon energy can be correlated to the ultraviolet photon energy. The excitation of surface plasmon by light is sometimes denoted as a localized surface plasmon resonance (LSPR) for the nanoscale metallic systems. The SPR is responsible for the bright red color of gold nanoparticles in the visible region of the electromagnetic spectrum. The SPR spectrum of the gold nanoparticles comprises of absorption and scattering of photons which depends on the size, shape and the surrounding environment. In metal nanoparticles, the surface polarization occurs due to the local field effect around the particles which cause the modification in their dielectric function. The response of the nanoparticles present in the medium can be described by Maxwell-Garnett dielectric function as follows;

$$\epsilon_{eff} = \epsilon_0 + 3N\epsilon_0 \frac{\epsilon_M - \epsilon_0}{\epsilon_M + 2\epsilon_0} \quad (1)$$

In equation (1), ϵ_M is the dielectric function of metal and N represent the density of particles. For resonance to occur the condition should be $\epsilon_M = -2\text{Re}(\epsilon_0)$ as shown in figure 1.1 [8].

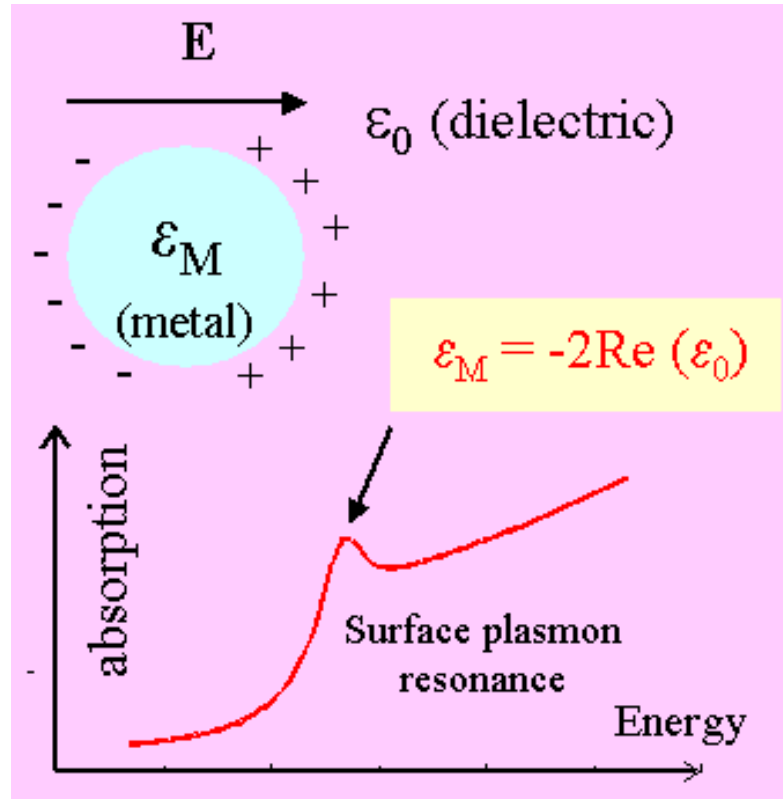


Figure 1.1 Surface Plasmon Resonance of Metal Nanoparticles

The SPR is very important to study the optical properties of gold nanoparticles. The characteristic SPR peak of gold nanoparticle occur between 525 nm and 530 nm. However, a shift in the SPR peak towards the higher wavelength region occurs with change in their shape from nanoparticle to nanorods. Furthermore, SPR is also widely employed to study the interaction of gold nanoparticles with biomolecules. The mobility of electrons in the presence of an electric field depends on the band gap of the material. In the case of a metal, the valence band and the conduction band overlap and the excited electron participate in the presence of an electric field as shown in Figure 1.2 [9].

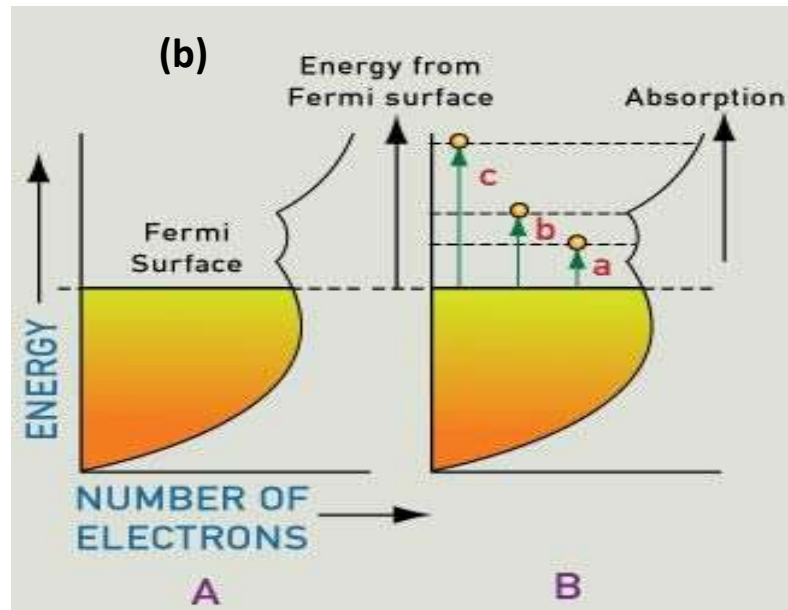
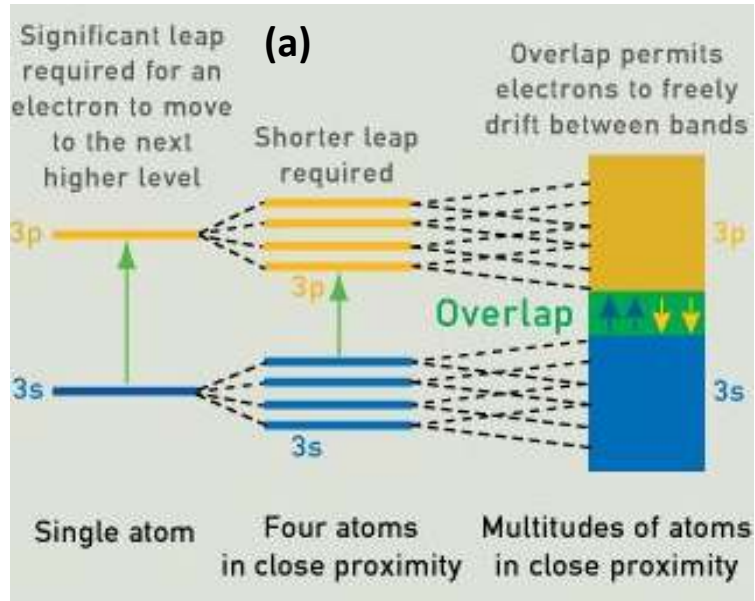


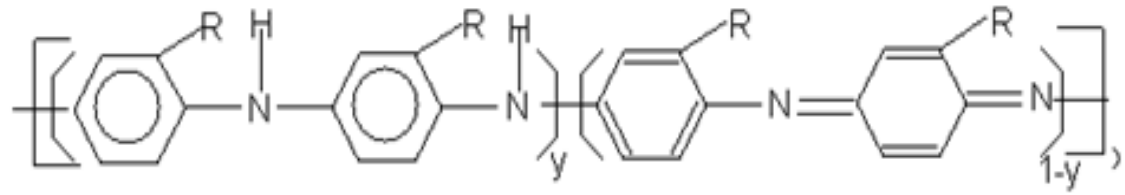
Figure 1.2 Schematic of the Overlapping of Energy Bands in Metal.

Figure 1.2(b) represents the Fermi level. Energy bands are empty at absolute zero temperature. The excitation of an electron from valence band to conduction band occurs

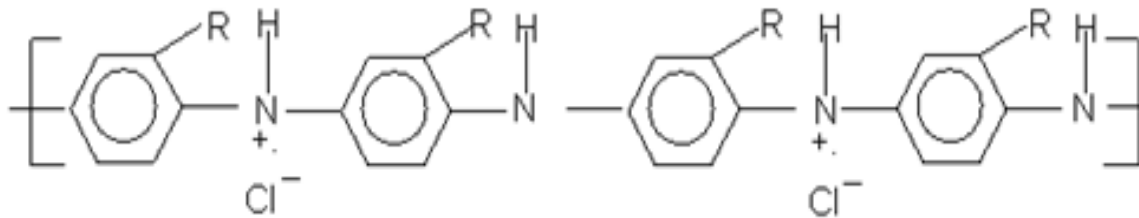
by the absorption of all the wavelengths of incident light by metal surface. Most of the incident light is immediately re-emitted at the surface, creating the metallic cluster as seen in gold, silver, and copper.

1.4 Composites of Polymer-Gold Nanoparticles

Recently, the applications of gold nanoparticles have been investigated extensively. Studies on conducting organic polymer material are gaining much attention in the area of sensors and molecular electronics [10-13] as described by Valter et al. [10], polyaniline, polypyrrole and polythiophene together with fullerenes are promising candidates for conducting organic polymers. According to Balazs et al. [14], the composites of polymers and the nanoparticles offer new opportunities for engineering flexible materials that display advantages in electrical, optical and mechanical properties. Of all available conducting polymers, Poly (o-anisidine) (POAS) and Polyaniline (PANI) has numerous applications in electronics, optical devices, biosensors and corrosion protection. The structure of the POAS is shown in figure 1.3. The structural, optical and electrochemical properties of this composite material of GNPs-POAS were studied by UV-Vis spectroscopy, TEM and Cyclic voltammetry.



(Emeraldine base)



(Emeraldine salt)

R = -H (Polyaniline)

= -OC₂H₅ (Poly(ortho-anisidine))

Figure 1.3 Schematic Representations of POAS in Emeraldine Base

Chapter 2: Experimental Methods

2.1 Introduction

The focus of this chapter is on the experimental approach and characterization techniques employed in this study. In this work, we have employed a chemical route for the synthesis of gold nanoparticles. In addition, we have also utilized various procedures for the shape selective nanoparticle synthesis and GNPs-POAS synthesis.

2.2 Materials

Hydroauric acid ($\text{HAuCl}_4 \cdot 3\text{H}_2\text{O}$), sodium citrate, PVP (poly vinyl pyrrolidone) and L-glutamic acid, Bovine Serum Albumin (BSA), Chitosan, N-methyl aniline, Chloroform, and Ammonium persulphate were all purchased from Sigma Aldrich(USA).

2.3 Synthesis of Gold Nanoparticles (GNPs)

In the literature, there are several methods available for the synthesis of gold nanoparticles [15-27]. However, in this work, we have employed only a few methods to synthesize the gold nanoparticles and are discussed below.

2.3.1 Citrate Reduction Method

This method involves the reduction of 0.01 M hydroauric acid (HAuCl_4) by citrate buffer. Briefly, 0.01 M HAuCl_4 (5mL) was mixed with DI water (100mL) and boiled.

Following this, 200 mg sodium citrate solution was added to the reaction mixture with constant stirring. The formation of gold nanoparticles will be complete when the color of the solution becomes wine red from its initial yellow color. The solution was further heated for additional 10 minutes.

2.3.2 Bio-Compatible Gold Nanoparticles

Biocompatible GNPs were synthesized using Chitosan as follows; initially, the GNPs were synthesized by the reduction of hydroauric acid (HAuCl_4) in L-glutamic acid. Briefly 0.01 M HAuCl_4 (5mL) is dissolved in DI water (50mL) and heated until it boils. Later, 10mL of 25mM L-glutamic acid is added to the reaction mixture with constant stirring. A color transition from yellow to red indicates the formation of gold nanoparticles. Following this, the solution was kept at room temperature. Next, 5mL of 1.0% chitosan was added to 20 ml of the gold solution with stirring and as a result the solution displayed a visible change in its color following chitosan addition.

2.3.3 Synthesis of GNPs Stabilized with Poly Vinyl Pyrollidone

In this method, we employ Poly-Vinyl-Pyrollidone (PVP) as a stabilizing agent for the GNP synthesis due to its excellent adsorption properties [16]. Gold nanoparticles in different shapes such as triangle, rectangle, pentagon and cubes can be synthesized using PVP. To achieve this, 1.0g of PVP was dissolved in 60mL of DI water and the solution was boiled. Later, 5mL of sodium citrate solution (prepared by mixing 647mg in 250mL of DI water) was added to the PVP solution in a hot plate and allowed to remain in the

hot plate for 10 min. Following this, HAuCl_4 (2.0 mL) was added to the solution with constant stirring.

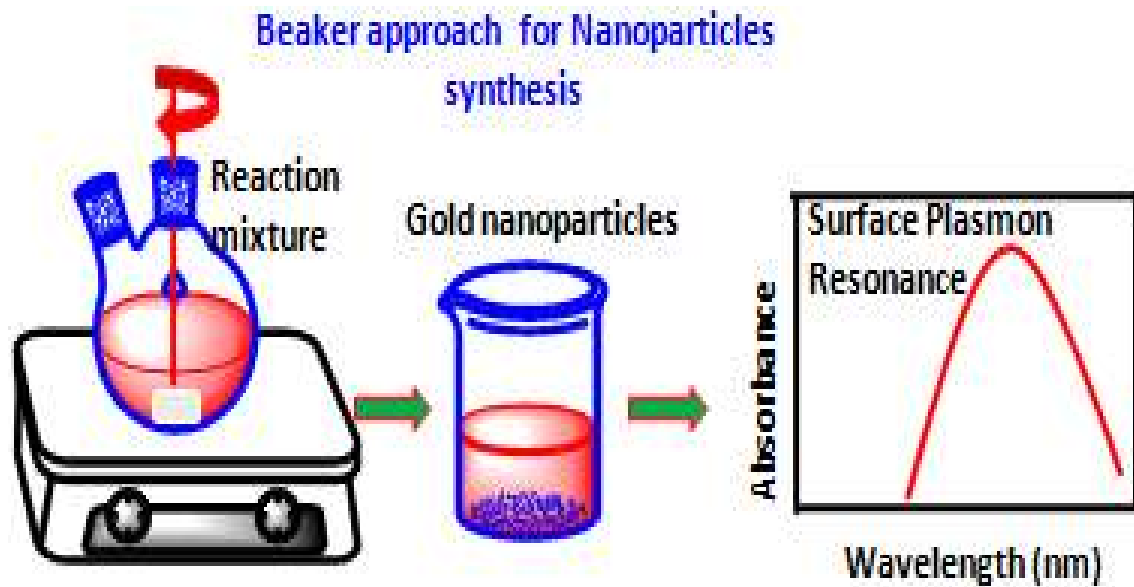


Figure 2.1 Schematic of the Chemical Assembly for Nanoparticles Synthesis

2.4. Synthesis of Composites of Polymer-Gold Nanoparticles

The synthesis of composite material was done by dissolving (0.2 M) of O-anisidine in 150 mL of 1.0 M HCl and the solution was kept aside for 1 hour. After an hour, 15 mL of 0.01 M HAuCl_4 was added to the above mixture with constant stirring for 10 minutes and kept aside (solution A) then 0.05 M ammonium persulphate solution was dissolved in 50 mL of 1.0M HCl with constant stirring for 15 min (solution B). After preparing these two solutions, solution B was added in drops to solution A at ice-cold condition and stored at room temperature for 24 hours. This resulted in the formation of a dark green precipitate. Next, the precipitate was filtered off and then washed subsequently with DI water and diethyl ether to remove all the oligomers. The resulting gold- POAS was dried at 100 °C.

The dried gold POAS powder was then dissolved in 1.0 M NaOH for 12 hours with subsequent washing in DI water and methanol (CH₃OH). The dark green powder thus obtained was the emeraldine base form of the GNPs-POAS conducting polymer [14].

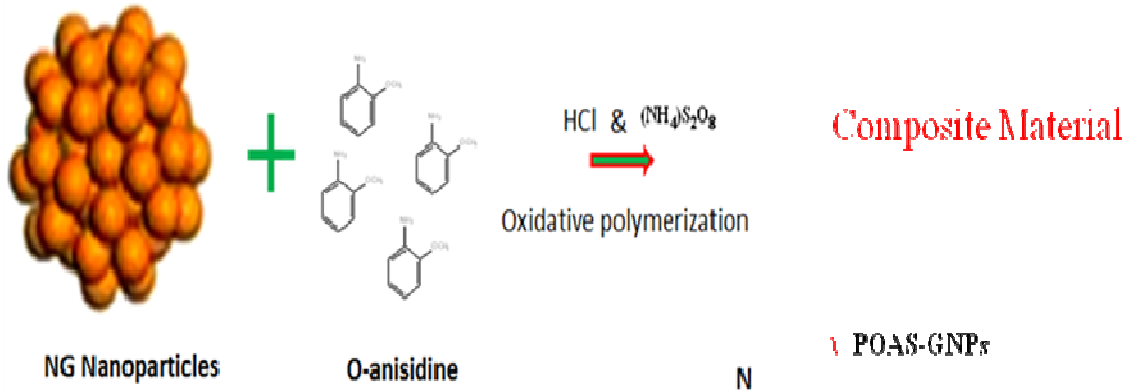


Figure 2.2 Schematic of the Oxidative Polymerization

2.5 Characterization Techniques

Various techniques employed for the characterization of GNPs were discussed in the following sections.

2.5.1 UV-vis Spectrophotometer

In UV-Vis spectrophotometer, interaction between sample (film, liquid solution or a solid material) and monochromatic light takes place resulting in the display of variables such as transmittance, reflectance and absorbance. UV/Vis spectrophotometer was employed in this work to study the absorption spectra and surface plasmon resonance (SPR) in gold nanoparticles. SPR spectroscopy is a highly sensitive technique often employed to study the optical properties of the metal nanoparticles and their sensitivity. The technique

requires a specialized set-up or arrangement which includes an electromagnetic radiation source generator, a dispersion device selecting a particular wavelength, a chopper dividing the path of light and a detector to measure the intensity of the radiation. Interaction between electromagnetic radiation and the surface plasmon at the particle interface and the surrounding medium results in the SPR phenomenon. Surface Plasmon refers to a collective oscillation of the conduction electrons present in the particle [4, 5] and as a result a strong absorption peak will be witnessed in the absorption region of metallic nanoparticles. For example, in the case of gold nanoparticles, its characteristic peak occurs at about 525 nm. The distinctive bright color of metal nanoparticle is attributed to the surface plasmon absorption band. [6] The SPR is very sensitive to the size and shape of the particles. Therefore, a small change in surface geometry affects the electrical density on the particle surface and causes them to oscillate with different frequency. This is due to the fact that, the optical properties of the metal nanoparticle is an intrinsic function of its morphological features [7]. Based on this, the absorption spectrum of the gold nanoparticles can be obtained between the 520 nm and 1000 nm range by tuning the geometry of the particle. In addition to the particle size and shape, the SPR peak is also sensitive to the dielectric properties of the surrounding medium [28].



Figure 2.3 UV-vis Spectrophotometer Set Up in USF

2.5.2 Transmission Electron Microscopy

Transmission electron microscopy (TEM) is the primary technique employed for determining the particle size, shape and the size distribution. TEM utilizes electron beam as light source that passes through all the lenses and apertures before reaching the specimen to be analyzed as shown in figure 2.4 [29]. The much lower wavelength makes it possible to get a resolution that is thousand times better than with a light microscope. TEM operates require electrons instead of light. In TEM, the electron gun emits the electrons and passes through the vacuum and then through a number of apertures and

electromagnetic lenses that focus the electrons into a very thin beam. This electron beam is then focused on to the object to be analyzed. The electrons get absorbed and reflected from the specimen depending on the density of the material and the transmitted electrons gives the magnified image of the specimen on a fluorescent screen. Figure 2.5 is a typical TEM employed in our work.

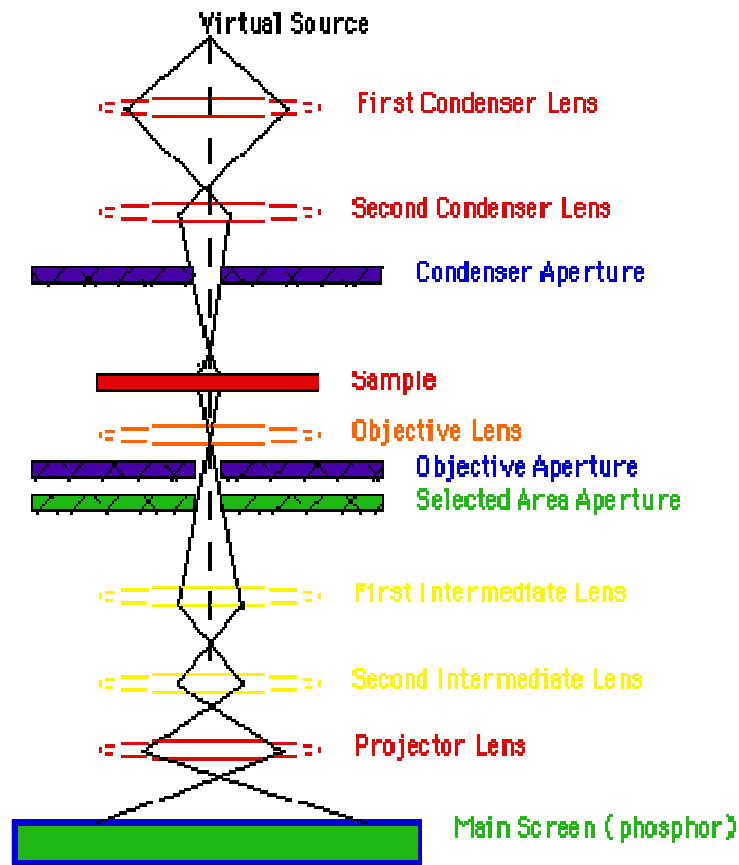


Figure 2.4 Optical Components in TEM



Figure 2.5 Schematic of Transmission Electron Microscopy in USF

2.5.3 Fourier Transform Infrared Spectroscopy

This technique is primarily used to identify the organic molecule or the presence of certain functional groups in the molecule. Infrared spectroscopy works in the IR region of the electromagnetic spectrum. When IR radiation is passed through a sample, the molecules absorb certain frequency of this radiation that is characteristic to their structure. The obtained spectrum then displayed the molecular absorption and transmission, and gives the molecular fingerprint of the sample. The different components of the IR spectroscope include an IR Source, Michelson Interferometer and a detector.

The advantage of IR spectroscopy is that it is very sensitive and a rapid technique for analyzing the composition of the given sample with better signal to noise ratio. Infrared spectrums gives information about the chemical bonding of the atoms, which is usually, represents by the absorption band caused by the vibration between the atomic bonds of the sample. Each material is composed of different combination of atoms, so different compounds produce different infrared spectrum. Therefore, infrared spectroscopy can result in a positive identification (qualitative analysis) of every different kind of material. In addition, the size of the peaks in the spectrum is a direct indication of the amount of material present [54].

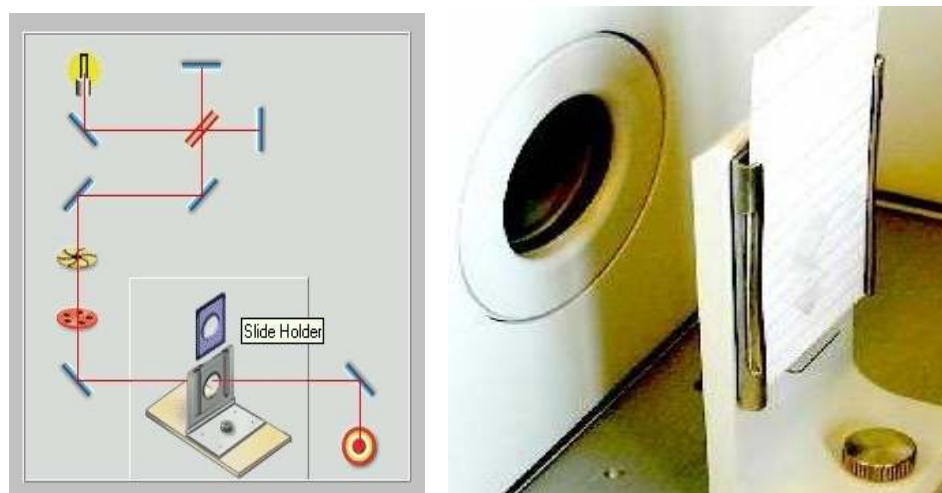


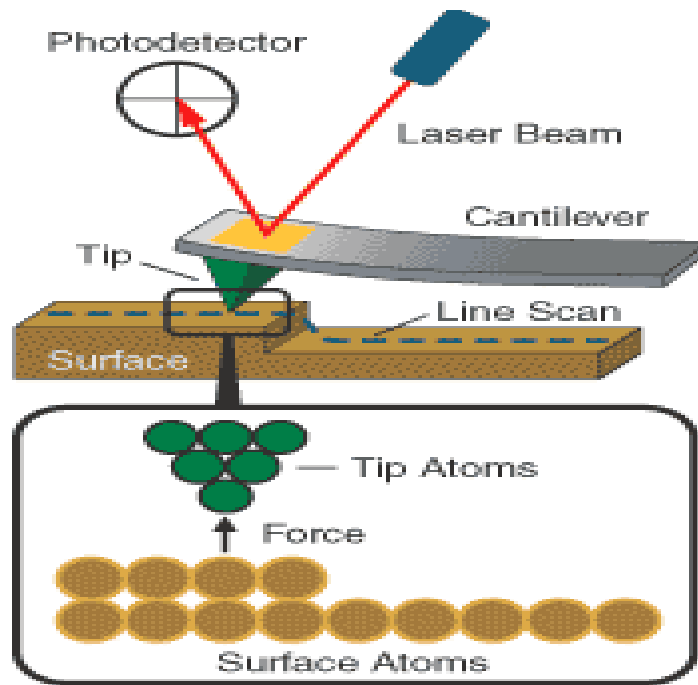
Figure 2.6 FTIR. Sample Holder, Sample Chamber

Figure 2.6 represents the schematic of the beam path in FTIR and the sample holder in the FTIR chamber [30].

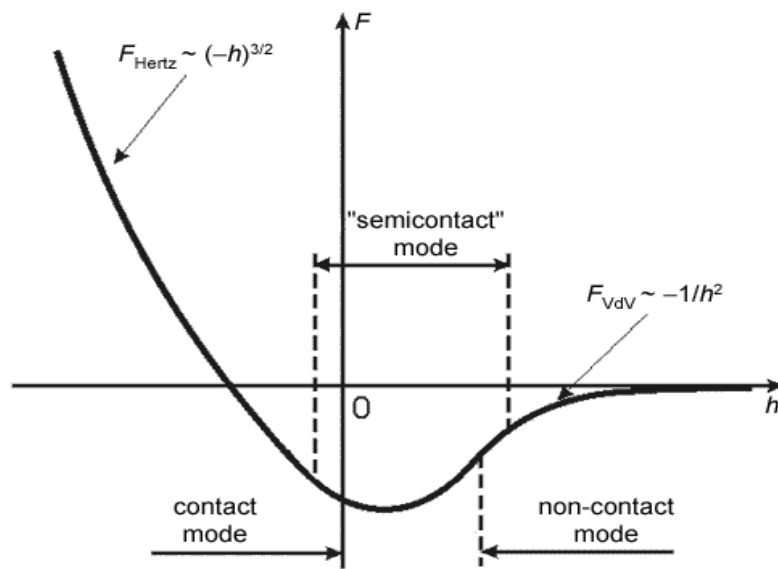
2.5.4 Atomic Force Microscopy

AFM is a technique used to analyze the surface of materials with magnifications up to 10^8 . It provides the three dimensional images from the conductive and non-conductive

sample with an extraordinary topographic contrast. An atomically very sharp silicon nitride tip connected to the end of the cantilever is used to scan the sample surface, while, maintaining the tip at constant height or force above the surface. The modes of operation in AFM include contact mode, non-contact mode and the tapping mode. In contact mode (also known as repulsive mode) the AFM tip come in close contact to the sample surface. The tip and the sample interact due to quantum mechanical exclusion principle. This mode gives the best resolution of the sample surface but the disadvantage of this mode is that it can deform the sample surface. In the non-contact mode, the cantilever vibrates at a certain distance (10 to 100 Å) and the topographical image is obtained by the Van-der Waals magnetic force with very poor resolution. In the tapping mode, the tip is brought close to the sample surface so that it cannot damage or deform the sample. The surface characteristics with resolution ranging from 100 μm to less than 1 μm can be accomplished by this technique. Figure 2.7 shows the schematic of the atomic force microscope mechanism of operation and different modes of operations [31]. In the present work, we employ the AFM techniques to probe the surface morphology of the gold nanoparticles.



(a)



(b)

Figure 2.7. Schematic of the Modes of Operation in AFM

2.5.5 Surface Enhanced Raman Spectroscopy

Surface-Enhanced Raman spectroscopy (SERS) is a technique to enhance the Raman signal magnitude by an order of 10^4 to 10^6 . This technique is mainly used to detect a molecular signal at a very low concentration and to study the surface of the material. Electromagnetic and chemical mechanisms are believed to be responsible for the SERS enhancement. Electromagnetic theory is based on the excitation of the surface plasmon, whereas, the charge transfer mechanism involves the bonding between the metal and the analyte and gives the chemical enhancement signal. Figure 2.8(a) represents the schematic of the nanoparticle based SERS and Figure 2.8(b) shows the Raman signal of the analyte in nanoshell (red) and SERS signal (blue) [32].

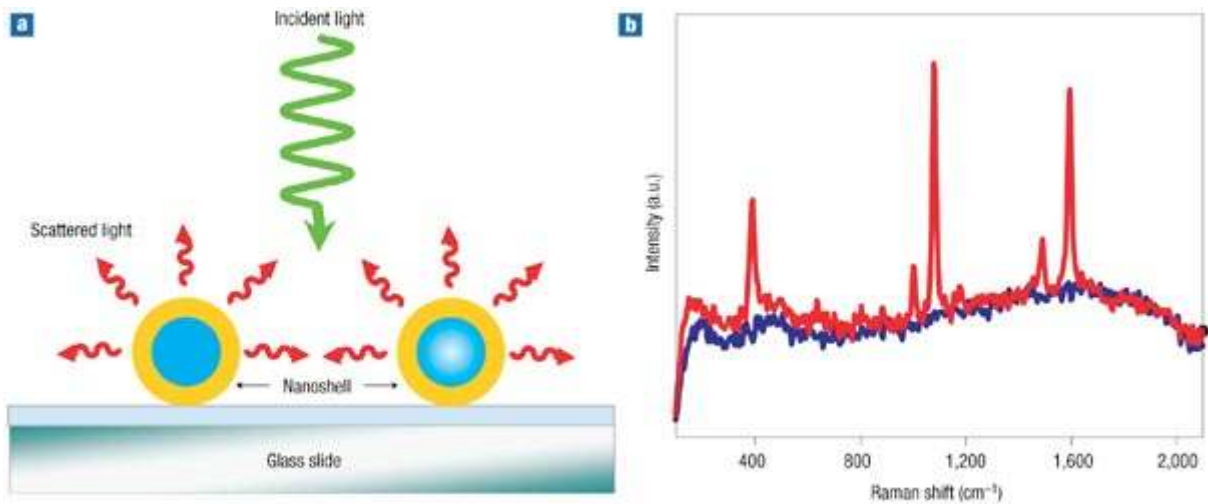


Figure 2.8 Schematic of Sample Geometry for Nanoparticle Based SERS

2.5.6 Electrochemical Voltammetry

Electrochemical voltammetry was usually performed in a three electrode electrochemical cell.

The three electrode system includes (a) a working electrode, (b) reference electrode and (c) an auxiliary electrode. The working electrode is the electrode at which our process of interest takes place and the auxiliary electrode is employed to complete the circuit. The reference electrode is used as reference against which the potential was applied or scanned between two limits. The surface area of the counter electrode must be high in order to achieve the impedance primarily from the working electrode. Usually, Platinum wire will be used as the counter electrode whereas gold, glassy carbon and platinum are used as working electrode. In the present work, we employ glassy carbon electrode modified with the gold nanoparticles as the working electrode, an Ag|AgCl reference electrode in all the electrochemical experiments.

2.5.6.1. Cyclic Voltammetry

A typical triangular voltage waveform applied to the working electrode during the cyclic voltammetric experiments is schematically represented in Fig 2.9 [33]. Here, the linear voltage is applied from t_0 and was steadily ramped until t_1 and at t_1 the ramp was reverted back to get the initial potential value at t_2 [33].

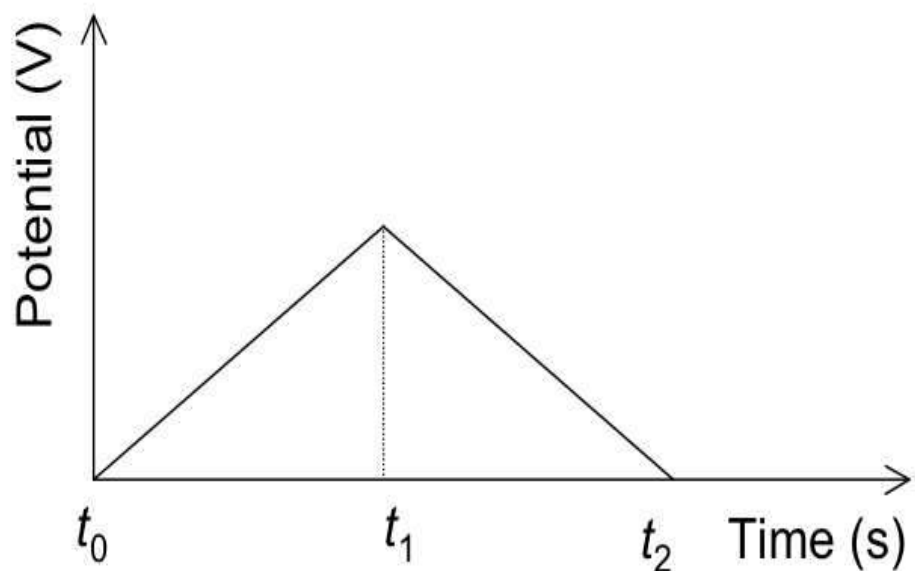


Figure 2.9 Typical Triangular Wave Form Applied to the Working Electrode.

Next, we briefly define a typical cyclic voltammogram in Figure 2.10 [33]. During cyclic voltammetry, the potential was scanned between two limits from the portion labeled A, until D and then reversed back to A. During this scan, a redox reaction will occur and this process will give rise to an increase in the current magnitude and this portion of the wave is called cathodic wave. Further, the maximum flow of electrons is observed at point C and after the point C, though the potential is applied, there will be no current observed beyond this due to the depletion of the redox species at the electrode. Further, the diffusion of the species toward the electrode should occur before reduction. In this case, the diffusion is slower than reduction and therefore there will be a decrease in the current flow between the points C and D. On the other hand, the points E, F, and G describe the reverse process. Furthermore, the redox potential can be obtained from a voltammogram by calculating the average value of the anodic and cathodic peaks. For example, for the

voltammogram shown in Fig.2.10, the one-electron ($E_{1,1/2}$) and two-electron ($E_{2,1/2}$) redox potentials can be calculated as:

$$E_{1,1/2} = (E_1^c + E_1^a) / 2 \text{ and } E_{2,1/2} = (E_2^c + E_2^a) / 2 \quad (1)$$

In equation (1), the subscript 1/2 represents the potential obtained approximately at the half-height of the cathodic and anodic peaks (and this is sometimes referred as half-wave potential). At these points the concentrations of the reduced and oxidized species are equal. However, it is to be noted that in this context concentration refers to the concentration of a given species on the electrode but not in the bulk solution. In certain cases, where only one-electron reduction occurs, only one maximum is observed in the cathodic wave and one minimum in the anodic waves. When both the anodic and cathodic waves are symmetric with respect to each other, the redox process is said to be reversible. However, if they are not symmetric, the redox species may undergo a chemical reaction and will not be observed during the reverse sweep [33].

Cyclic voltammetry is a commonly employed electrochemical technique, during which the potential of the working electrode is ramped in a linear fashion versus time. After reaching the initial potential, the potential of working electrode is reversed and is called one cycle. Cyclic voltammetry can be performed for a single cycle or a series of cycles depending on the sensitivity as required by the analysis. A plot of the current magnitude at the working electrode versus the applied voltage will give rise to a cyclic voltammogram. Furthermore, the utility of cyclic voltammetry is strongly dependent on the analyte being employed and the analyte has to be redox active within the applied potential range.

The redox reaction at the surface of the working electrode will certainly bring about a mass transfer of the material at a definite applied voltage. The advantages of the cyclic voltammetry include highly sensitivity to the traces of ionic species, non-destruction and can be employed at a wide dynamic range.

In the present work, gold nanoparticles of different sizes and shapes were employed as a substrate for all the voltammetric measurements in different redox probes such as hexammineruthenium (III) chloride, and potassium ferricyanide. Further, these electrodes modified using gold nanoparticles were then employed for the detection of neurotransmitters such as dopamine and ascorbic acid.

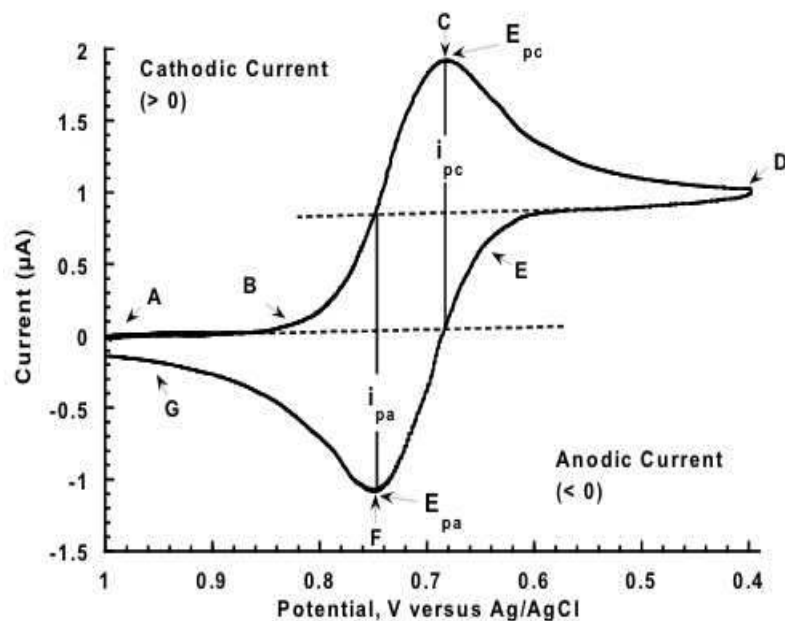


Figure 2.10 A Typical Cyclic Voltammogram of One Electron Transfer

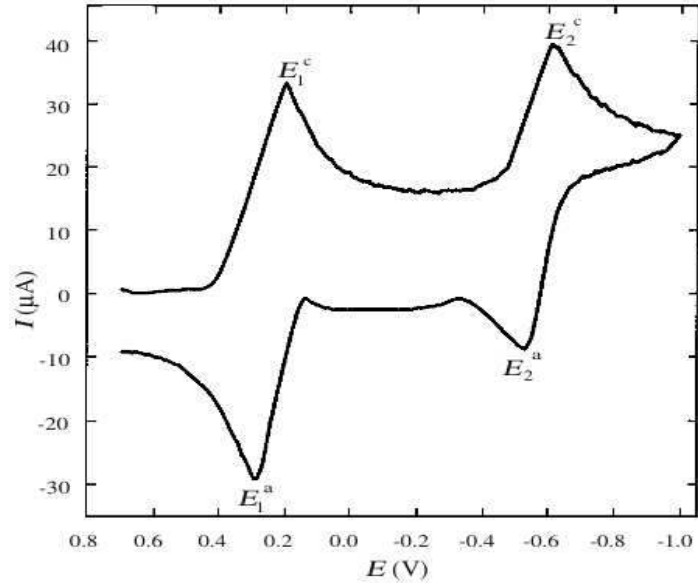


Figure 2.11 Typical Cyclic Voltammogram of Two Electron Transfer

In the present work, gold nanoparticles of different sizes and shapes were employed as a substrate for all the voltammetric measurements. Two different redox probes such as hexammineruthenium (III) chloride and potassium ferricyanide has been utilized for the experiment. Further, these electrodes modified using gold nanoparticles were then employed for the detection of neurotransmitters such as dopamine and ascorbic acid.

Chapter 3: Structural and Optical Properties of Gold Nanoparticles

3.1 Introduction

The structural and optical properties of gold nanoparticles synthesized by the chemical route were described in this chapter. The main focus of this chapter is to characterize the GNPs. Synthesis of GNPs at different conditions (such as temperature, reducing agent and concentration) results in the variation of gold nanoparticles morphology which in turn displays a remarkable difference in the optical properties. The characterization of the composites of gold nanoparticles-POAS was studied using UV-Vis, TEM, FTIR and cyclic voltammetry.

3.2 Characterization of Au Nanoparticles

Gold nanoparticles were studied by different techniques discussed below.

3.2.1 Absorption Spectroscopy

The absorption spectra of gold nanoparticles were obtained using UV-vis spectrophotometer. This measurement was performed using the gold nanoparticle solution within the quartz cell along with the reference cell. The characteristic plasmon resonance absorption band for GNPs occurs at 525 nm in the visible region of the electromagnetic spectrum. Figure 3.1 shows the absorption spectra of 20nm gold nanoparticles with surface plasmon resonance band at 529 nm. It is well known that the

optical properties of metal nanoparticles are strongly dependent on the morphology of the nanoparticles [16]. The size analysis of the GNPs was performed by visually analyzing the color of the nanoparticle solution. The color transition from deep red to bluish purple indicates the formation of bigger particle due to SPR properties of the gold nanoparticles. The SPR properties of the nanoparticles were displayed in the visible region of the electromagnetic spectrum [34] When the nanoparticles are exposed to the electromagnetic radiation, a part of the wavelength get absorbed and a portion of it were reflected by these particles and the remaining reflected portion of the wavelength was responsible for the intense bright color of the nanoparticles.

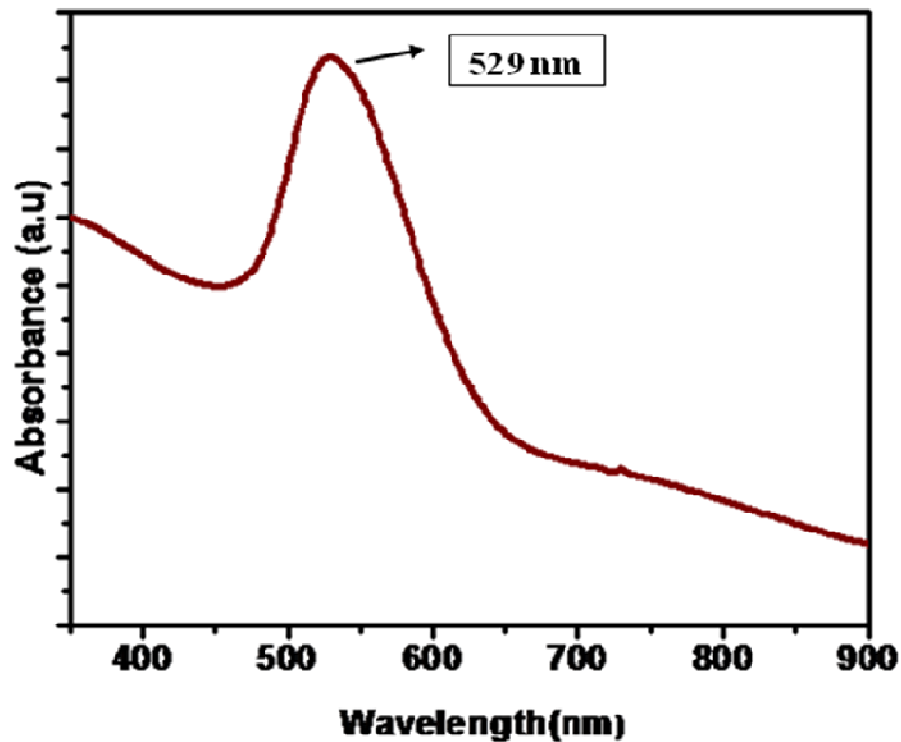


Figure 3.1 Absorption Spectrum of the Gold Nanoparticles

Figure 3.2 represents the absorption spectra obtained for the gold nanoparticles synthesized by the citrate reduction method. The variation in the absorption spectra is due to the particle size variation, which is determined by amount of sodium citrate being used. As the size of particle increases the SPR displays red shift. Figure 3.3 represents different gold nanoparticle solutions. All the nanoparticles are synthesized chemically. As the size of gold nanoparticles increases the solution of gold nanoparticles displays remarkable changes in the color from red to purple.

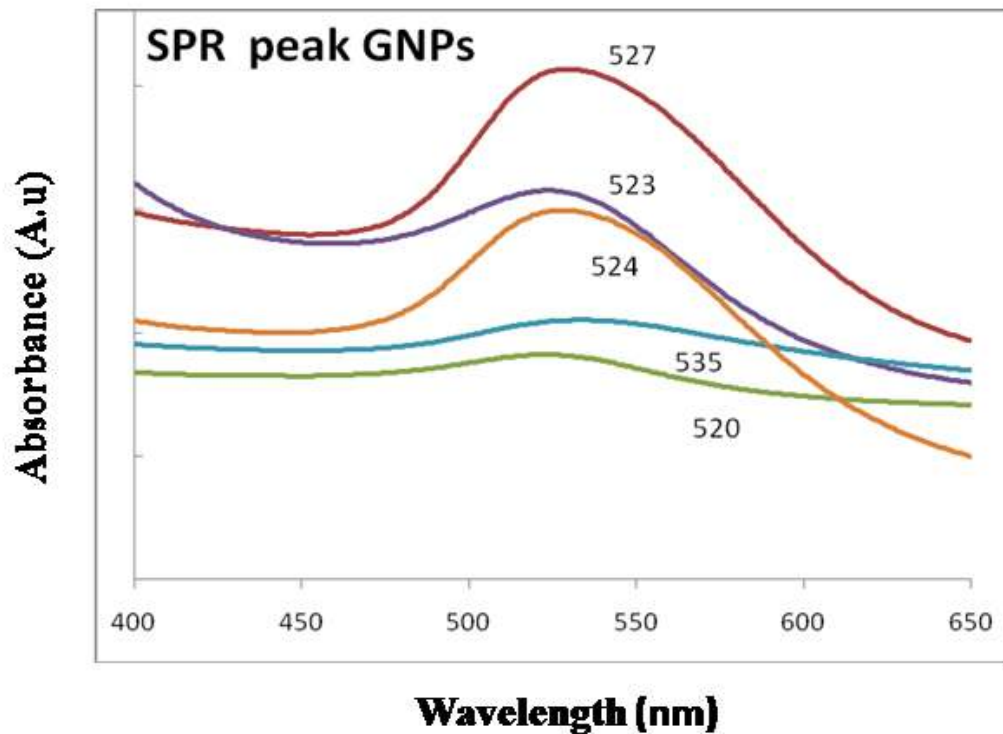


Figure 3.2 UV-Visible Absorption Spectrum of the Gold Nanoparticles Synthesized by Citrate Reduction Method.



Figure 3.3 Images of Gold Nanoparticle Solutions

Figure 3.3 represents the images of different gold nanoparticles Solutions which is directly related to the size of gold nanoparticles. Figure 3.4 represents the absorption spectrum of the gold nanoparticles synthesized by using PVP with size ranging from 10 nm to 60 nm. Further, it displays remarkable variation in the surface plasmon band, since the optical behavior of the gold nanoparticles was based on the shape and size of GNPs [16]. Furthermore, the surface plasmon peak shifts towards the higher wavelength as the shape and size of the GNPs varies from nanosphere to nanooctagon.

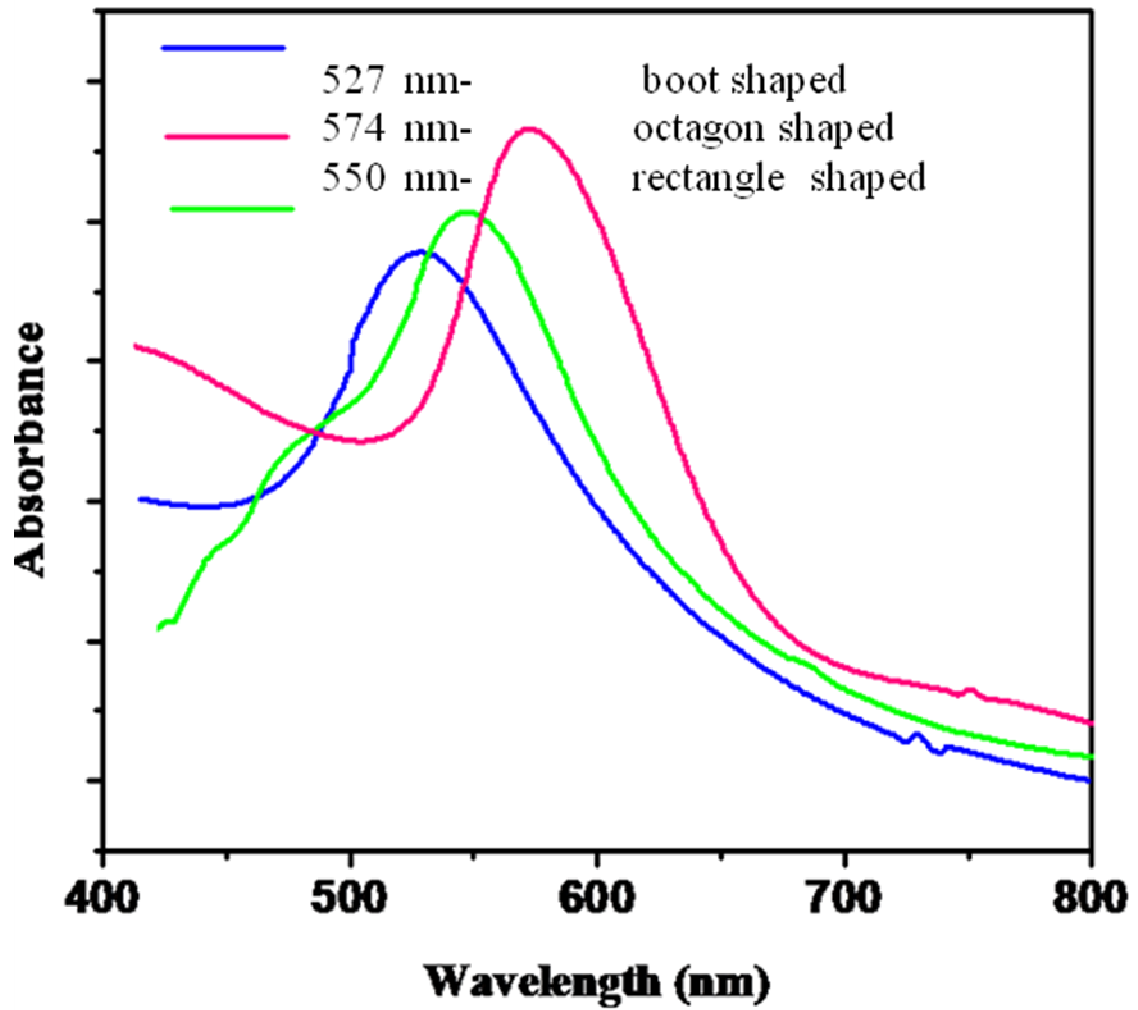


Figure 3.4 Absorption Spectra of Gold Nanoparticles (~527 nm, 550 nm and 574 nm.)

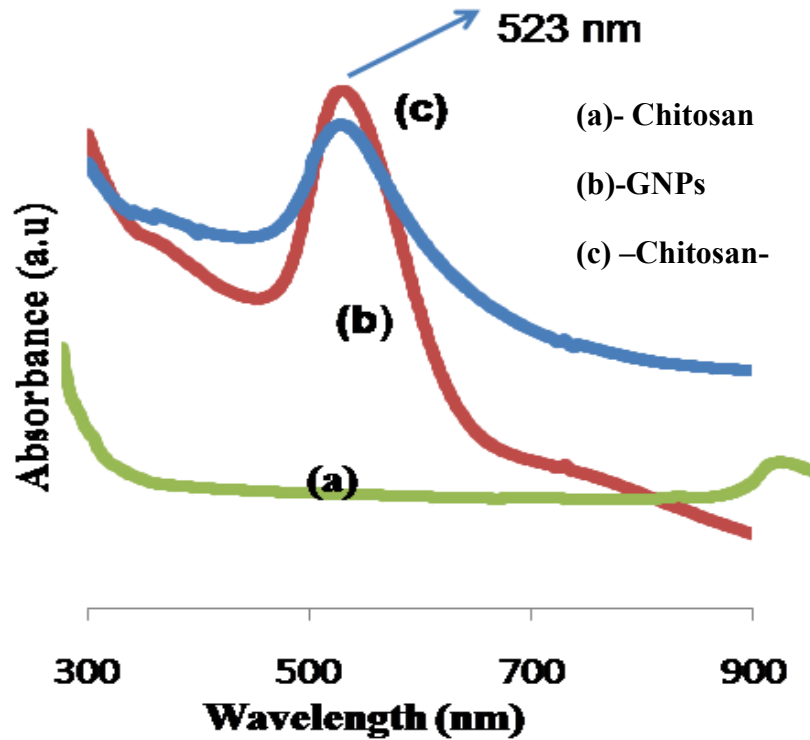


Figure 3.5 UV-vis Spectra of Bio-Compatible Gold Nanoparticles.

As shown in the figure 3.5 the absorption spectra of gold nanoparticles synthesized by using chitosan as a stabilizing agent act as biocompatible since chitosan is a bio-polymer and responsible for the transportation of some biological objects including some drugs. Since chitosan does not show any optical activity so the observed change in the SPR band of GNPs (523 nm) after the addition of chitosan is due to the change of the dielectric variation [35].

3.2.2 Morphology Analysis of GNPs (TEM)

Transmission Electron Microscope was used to study the morphology of gold nanoparticles. A drop of the GNPs solution is casted on the TEM grid and allowed to dry in air before performing the TEM measurement. Further, care must be taken in order to

avoid the excessive spill of organic surfactant on the GNPs sample; otherwise, it will be difficult for the electron beam to pass through the sample that surrounds the nanoparticles. The morphology of the GNPs is characterized by the transmission electron microscopy. TEM images of some samples of gold nanoparticles obtained chemically were shown below. Figure(s) 3.6, 3.7, 3.8, 3.9 and 3.10 are the TEM images of the gold nanoparticles synthesized by citrate reduction method and appear to be boot shaped and spherical in shape with an average size about of 20 nm and ~500 nm. Figure 3.11, 3.12 and 3.13 represents the TEM images of the nanoparticles synthesized by using PVP and resembles pentagon, triangle and octagon with a size range from 20 nm to 200 nm. It is evident from the TEM study that the nanoparticles of different sizes and shape can be obtained *via* the chemical synthesis.

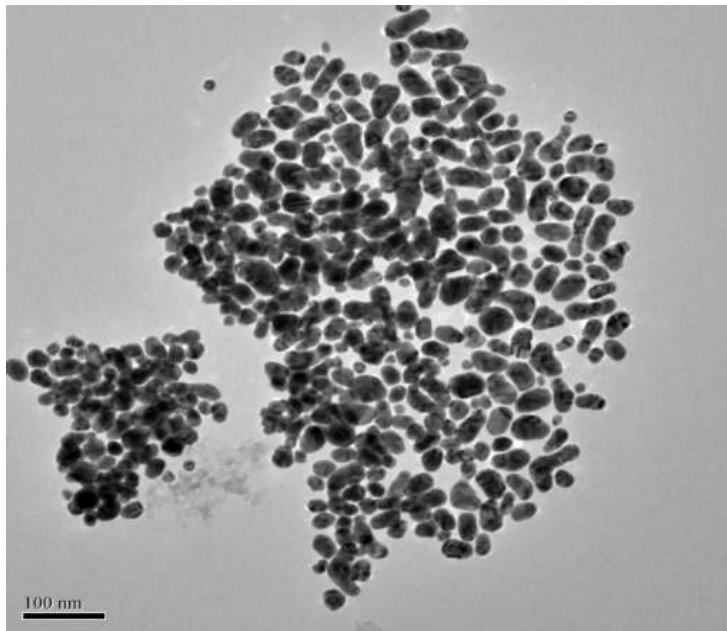


Figure 3.6 TEM Images of the Gold Nanoparticles (Boot Shaped)

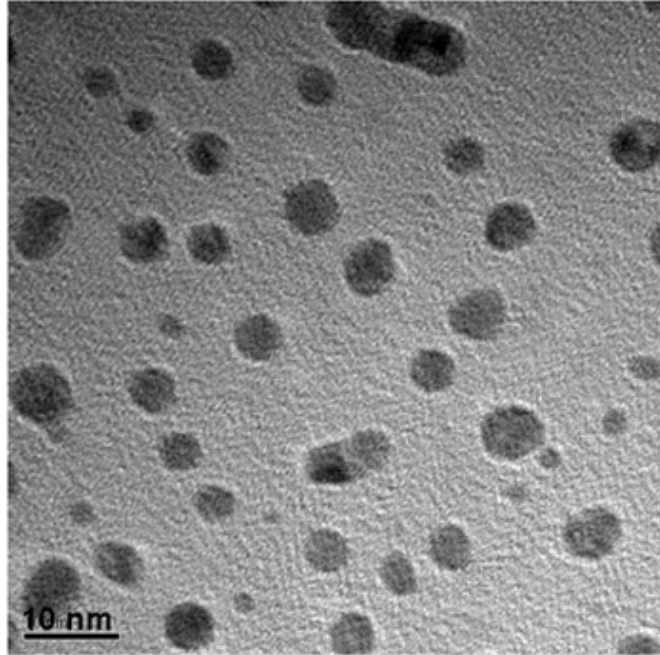


Figure 3.7 TEM Images of GNPs (~5 nm-7 nm)

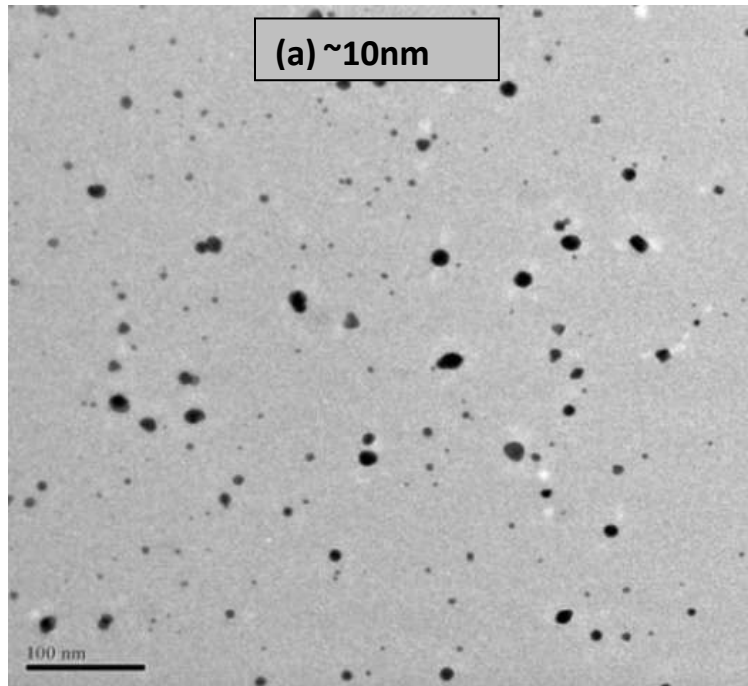


Figure 3.8. TEM Images of GNPs (~10 nm)

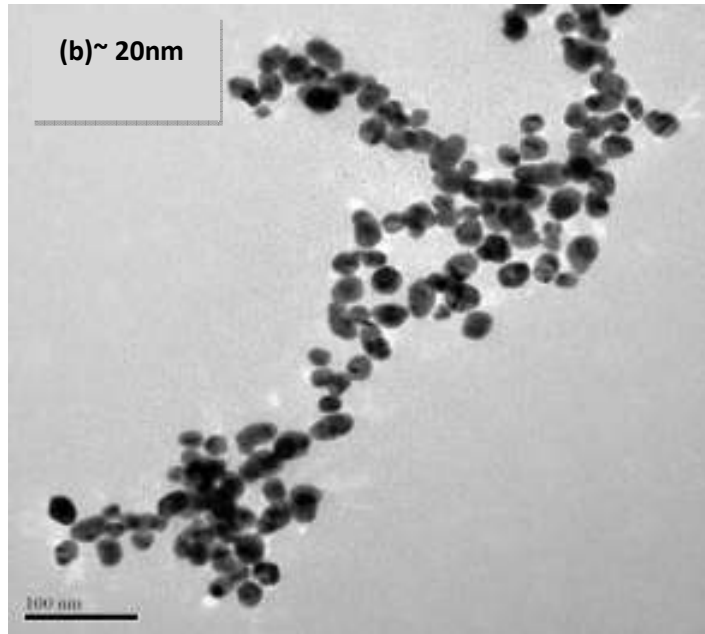


Figure 3.9 TEM Images of GNPs (~20 nm)

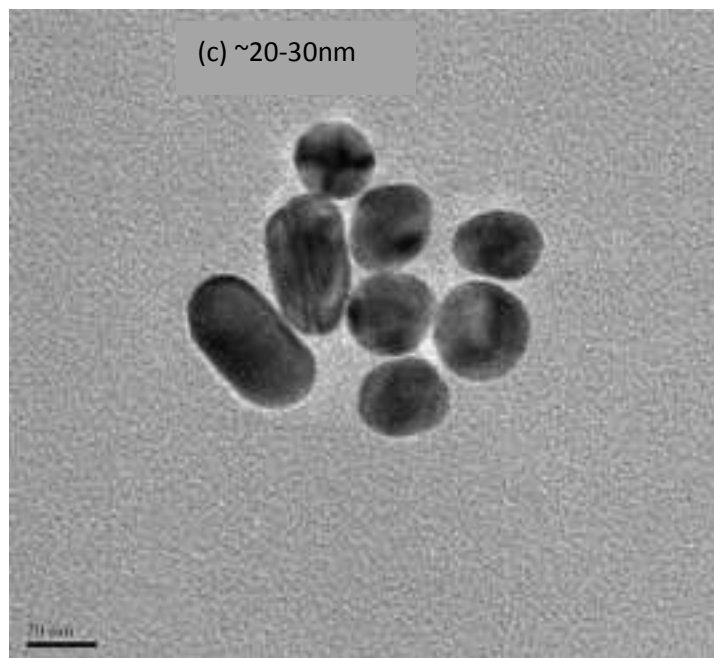


Figure 3.10 TEM Images of GNPs (~20 nm-30 nm)

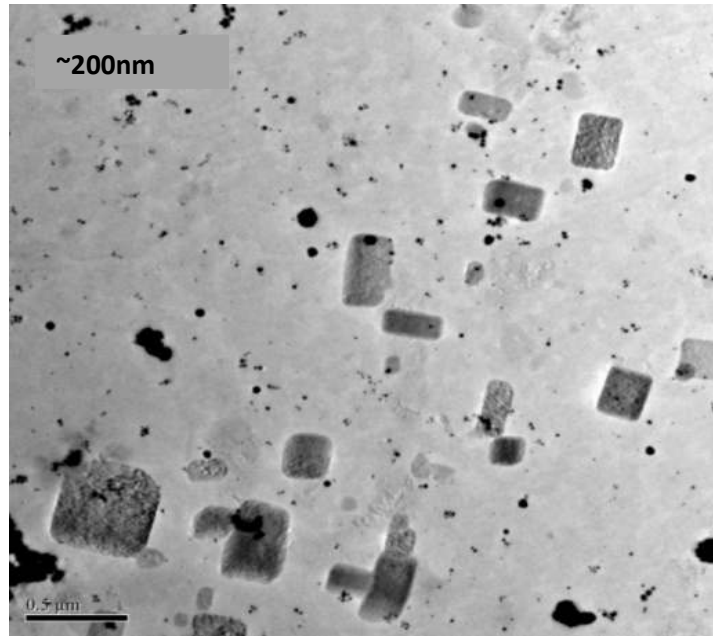


Figure 3.11 TEM Images of GNPs Nanocubes (~200nm)

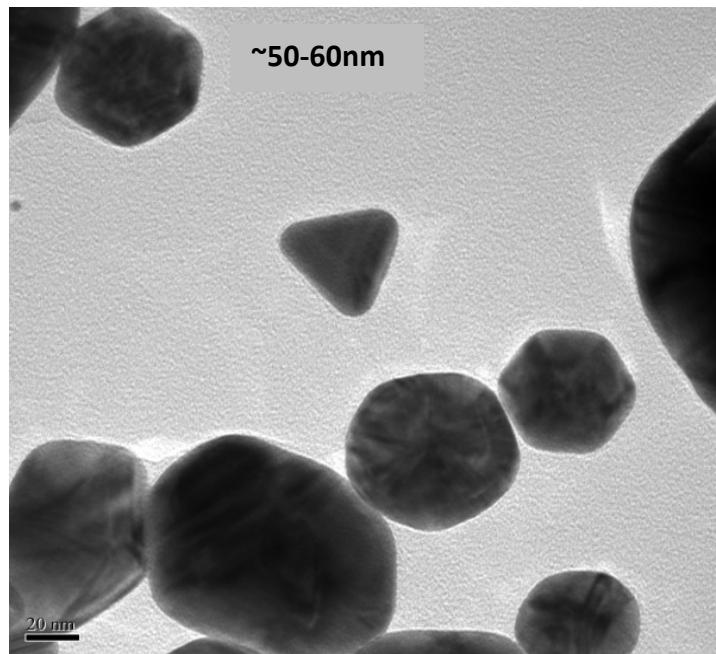


Figure 3.12 TEM Images of GNPs (Nanotriangles, Octagons~50 nm-60 nm)

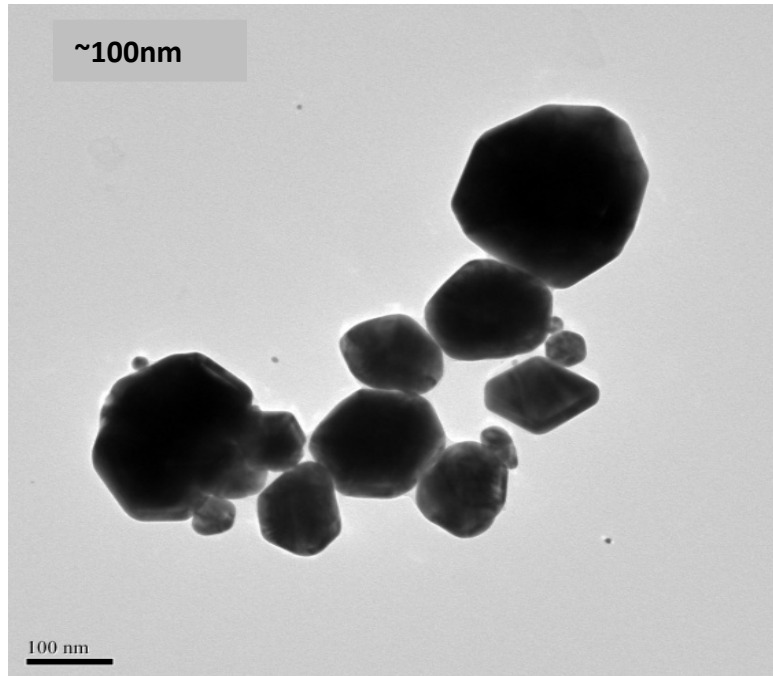


Figure 3.13 TEM Images of GNPs (Cubes, Pentagon ~ 100 nm).

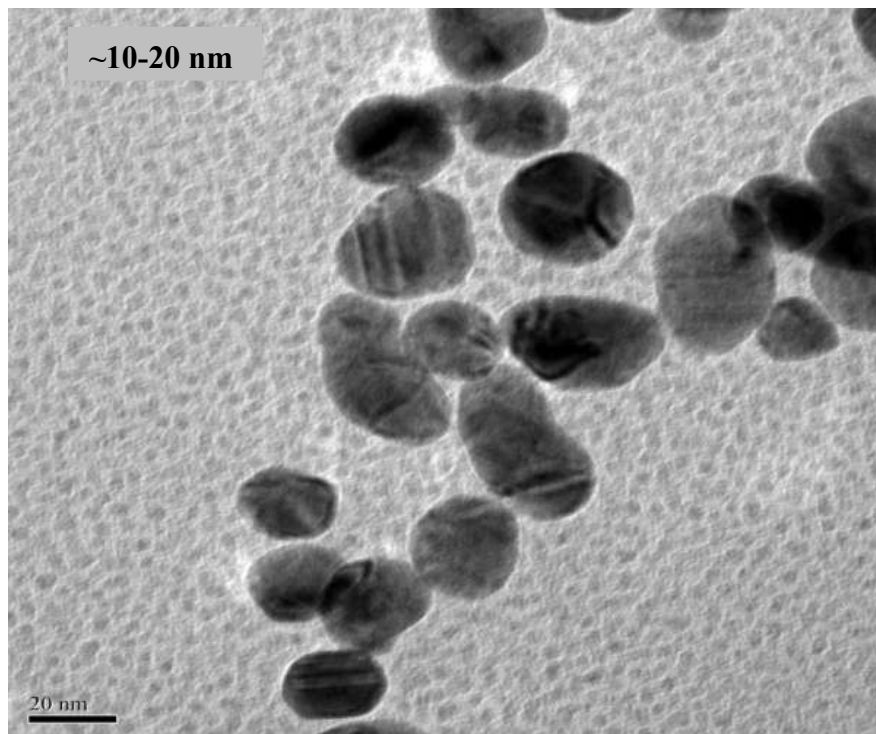


Figure 3.14 TEM Image GNPs (~10 nm-20 nm)

The following table shows the different parameters utilized during the synthesis of gold nanoparticles and resulting nanostructure size.

Table 3.1. Gold Nanoparticles: Synthetic and Characterizing Parameters

<i>Volume of (0.01M) H₂AuCl₄</i>	<i>Concentration of Sodium citrate</i>	<i>PVP (gm)</i>	<i>L abs max (nm)</i>	<i>Size (nm)</i>
<i>10ml</i>	<i>647/250ml DI</i>	<i>1gm/60ml</i>	<i>550nm</i>	<i>50-100nm</i>
<i>10 ml</i>	<i>400mg/100ml DI</i>	<i>0</i>	<i>514nm</i>	<i>~7to 10nm</i>
<i>15 ml</i>	<i>340 mg/100ml DI</i>	<i>0</i>	<i>526nm</i>	<i>10nm</i>
<i>15 ml</i>	<i>320 mg/100 ml DI</i>	<i>0</i>	<i>525nm</i>	<i>10 ~20nm</i>
<i>10 ml</i>	<i>300 mg/ 250 ml DI</i>	<i>0.8gm/60ml</i>	<i>574nm</i>	<i>500nm</i>

3.2.3 SERS

The SERS of the gold nanoparticles shows peak enhancement of the material present in a tiny amount of sample. The SERS of different samples of gold nanoparticles was performed in the Argon/Krypton Laser (HORIBA JOBINYVON). The wavelength employed in this work was 647 nm, a 20x objective in 3 acc operational mode. The experiment was performed by irradiating the solution of gold nanoparticles with the laser light and the results were recorded by a spectrum of the scattered light. The optical properties of the nanoparticles affect the scattering of the light which gives the characteristic vibration fingerprint of the molecules present. As described by the Hu's group [17], the SERS intensity of the nanoparticles was strongly dependent on the morphological features. As the sharp edges within the nanoparticles increases, the SERS activity increases too. Our SERS characterization results indicated that the bigger

nanoparticles like pentagon, triangles and octagon showed intense SERS activity than the smaller spherical particles. The SERS of the protein adsorbed on the different sized nanoparticles and shape produce different SERS frequency, which gives the idea of the protein-nanoparticles interaction [17, 18].

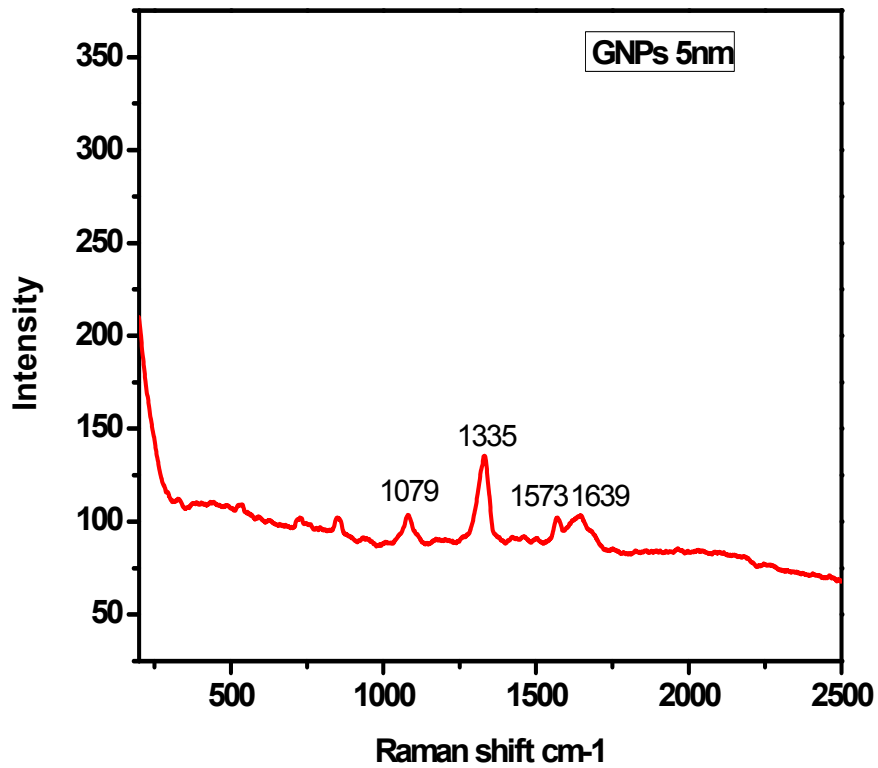


Figure 3.15. SERS of 5 nm Gold Nanoparticles

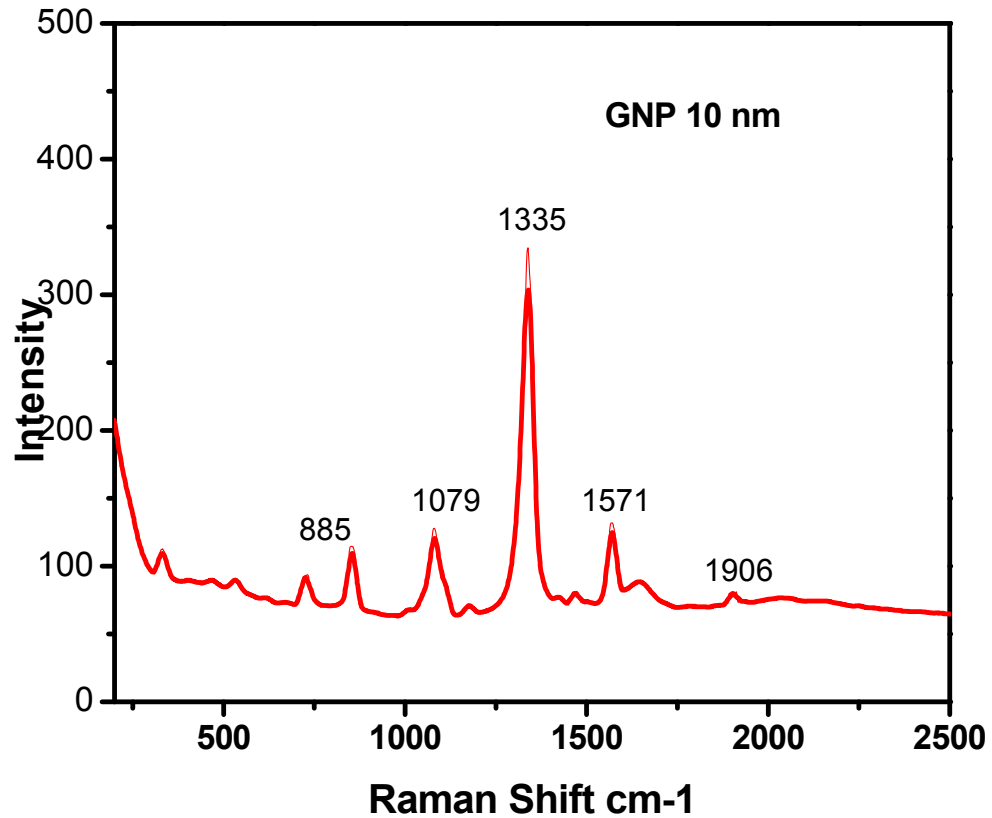


Figure 3.16 SERS of 10 nm Gold Nanoparticles

SERS analysis of different sized gold nanoparticles (7nm, 10nm, 20 nm) has been performed in this work. The SERS of these three samples of gold nanoparticles displayed main peaks at 885 cm^{-1} (NH_2), 1079 cm^{-1} (C–C and C–N stretch), 1335 cm^{-1} ($\text{NH}_2\text{--CH}_2$ twist) and $1573\text{--}1599\text{ cm}^{-1}$ for --COOH asym as shown in figure 3.16. Further, the SERS of gold nanoparticle sample displayed reproducible spectra with variations in peak intensity (intensity varies between 7 nm and 20 nm)

3.2.4 Atomic Force Microscopy

Next, the surface morphology of the gold nanoparticles was studied by AFM under tapping mode. The AFM micrograph in 2D is shown in figure 3.17.

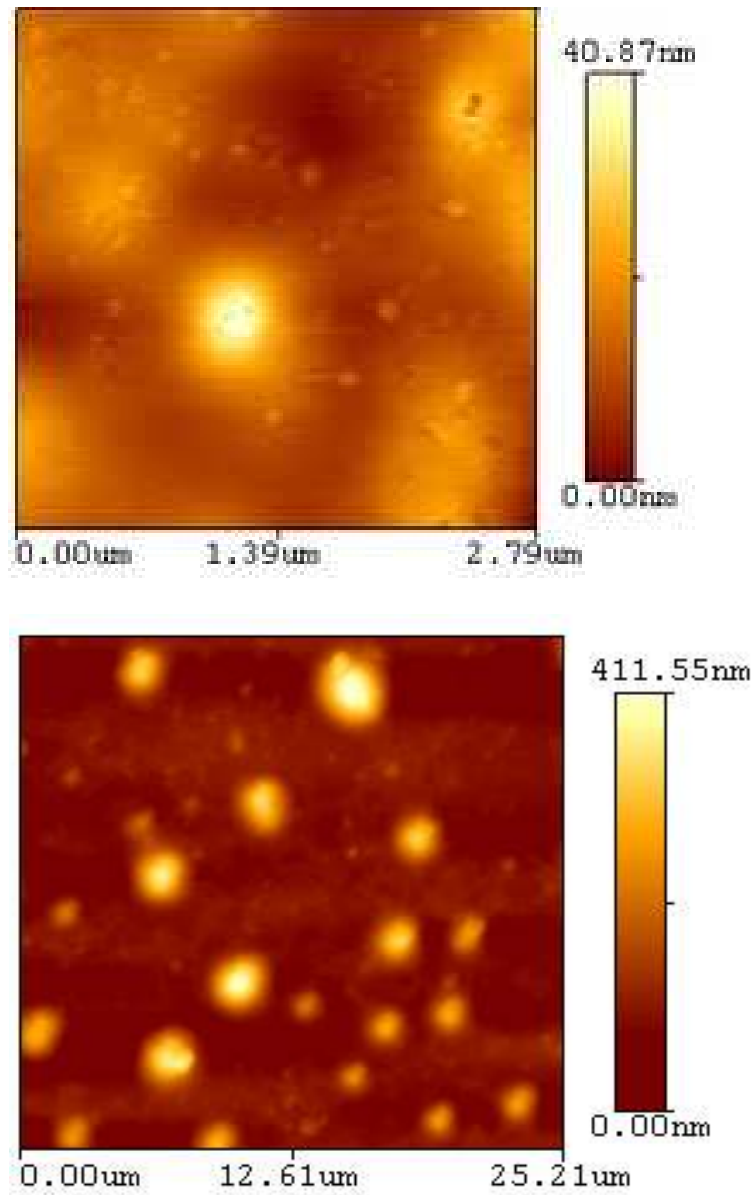


Figure 3.17 AFM Images of Gold Nanoparticles

3.2.5 Electrochemical Characterization of GNPs

Cyclic voltammetric experiments were performed in an electrochemical cell containing a three electrode assembly. Gold nanoparticles were immobilized on the glassy carbon electrode and employed as the working electrode, platinum wire as the auxiliary electrode, and Ag/AgCl/saturated with 3.0M KCl was employed as the reference electrode. Initially, cyclic voltammetric experiments were performed using $[K_4Fe(CN)_6]^{3-/4-}$ (a negatively charged redox probe) and $[Ru(NH_3)_6]^{3+/2+}$ (a positively charged redox probe). Figure 3.18 and 3.19 represents the background subtracted cyclic voltammogram obtained at a glassy carbon electrode modified with 20 nm GNPs immobilized on to a glassy carbon electrode in 1.0mM $[Ru(NH_3)_6]^{3+/2+}$ / 0.5M KCl and 1.0mM $K_3Fe(CN)_6^{3-/4-}$ / 0.5M KCl respectively. The CV of GNPs in $[Ru(NH_3)_6]^{3+/2+}$ exhibited a reduction and oxidation peak centered at 0.14V and 0.08V respectively with a ΔE_p value of 60mV confirming a one-electron transfer. On the other hand, the cyclic voltammetry of GNPs in $[K_3Fe(CN)_6]^{3-/4-}$ exhibited reduction and oxidation peaks centered at 0.42V and 0.36V respectively with a ΔE_p value of about 60mV indicating a one electron transfer. From these experiments, it was evident that the gold nanoparticles (20nm) provides an effective platform for the electron transfer to occur thereby confirming the suitability of the nanoparticles as a sensing platform for various bioanalysis.

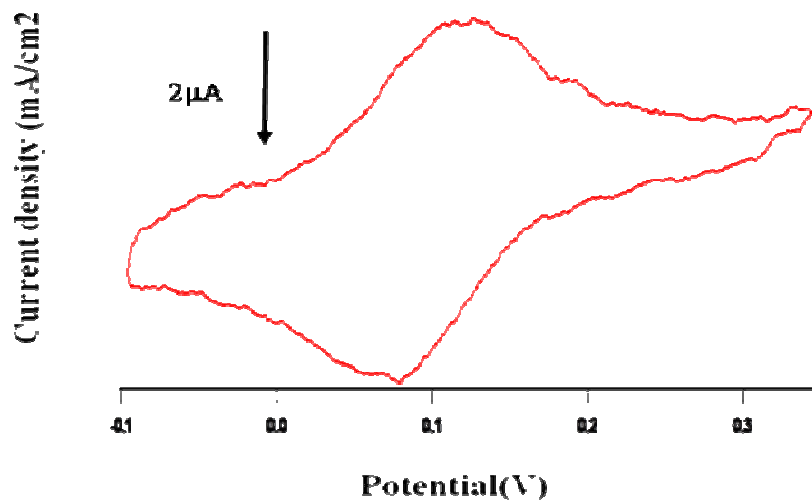


Figure 3.18 C.V of GNPs 20 nm.E|V vs. Ag|AgCl in $[\text{Ru}(\text{NH}_3)_6]^{3+/2+}$

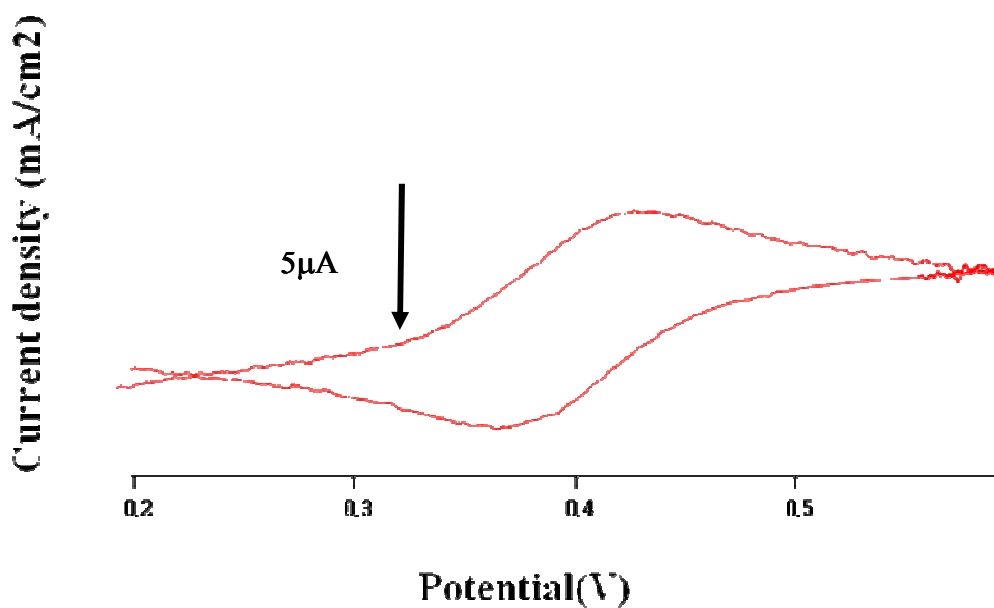


Figure 3.19 C.V of GNPs 20nm.E|V vs. Ag|AgCl in $[\text{K}_4\text{Fe}(\text{CN})_6]^{3-/4-}$

3.3 Characterization of Gold-Polymer Composites

The characterization techniques employed for the study of POAS-GNPs nanocomposites includes UV-Vis, TEM and SERS. Further, the electrochemical properties were also

studied in detail in the next section. The UV-Visible spectra of the composite materials deposited on the quartz substrate were recorded by a UV-Vis spectrophotometer. Figure 3.20 and 3.21 shows the optical spectrum of the GNPs and GNPs-POAS. The characteristic peaks of POAS were positioned at 330 nm ($\pi-\pi^*$ transition) and at 610 nm ($n-\pi^*$ transition). In addition, a peak was observed at ~ 500 to 550 for the GNPs-POAS composite due to the presence of gold nanoparticles in the POAS matrix.

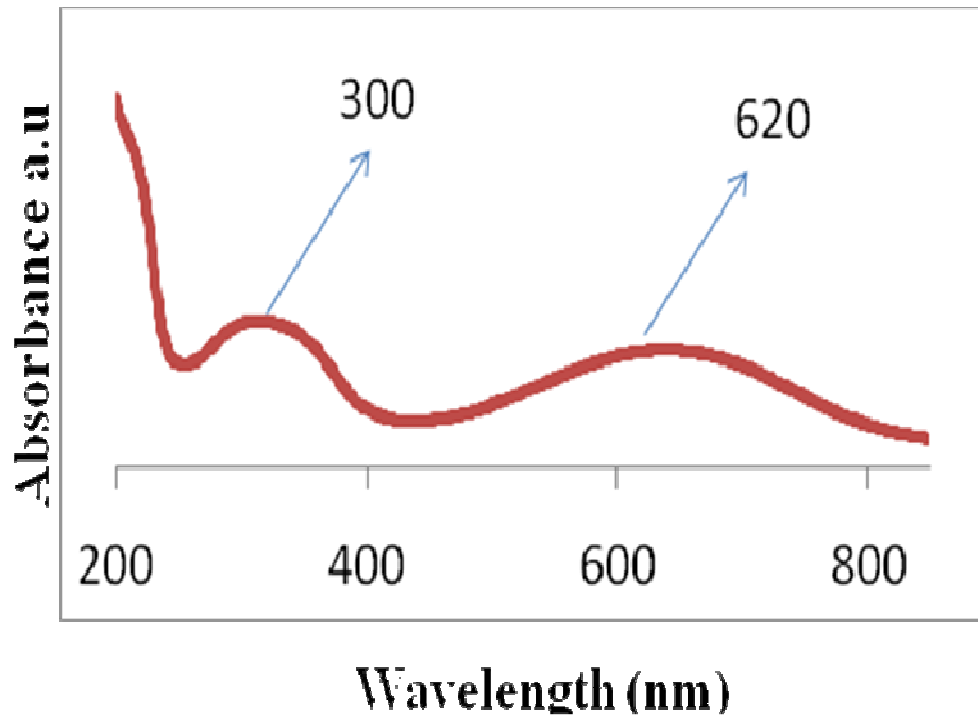


Figure 3.20 UV-vis Spectra of POAS

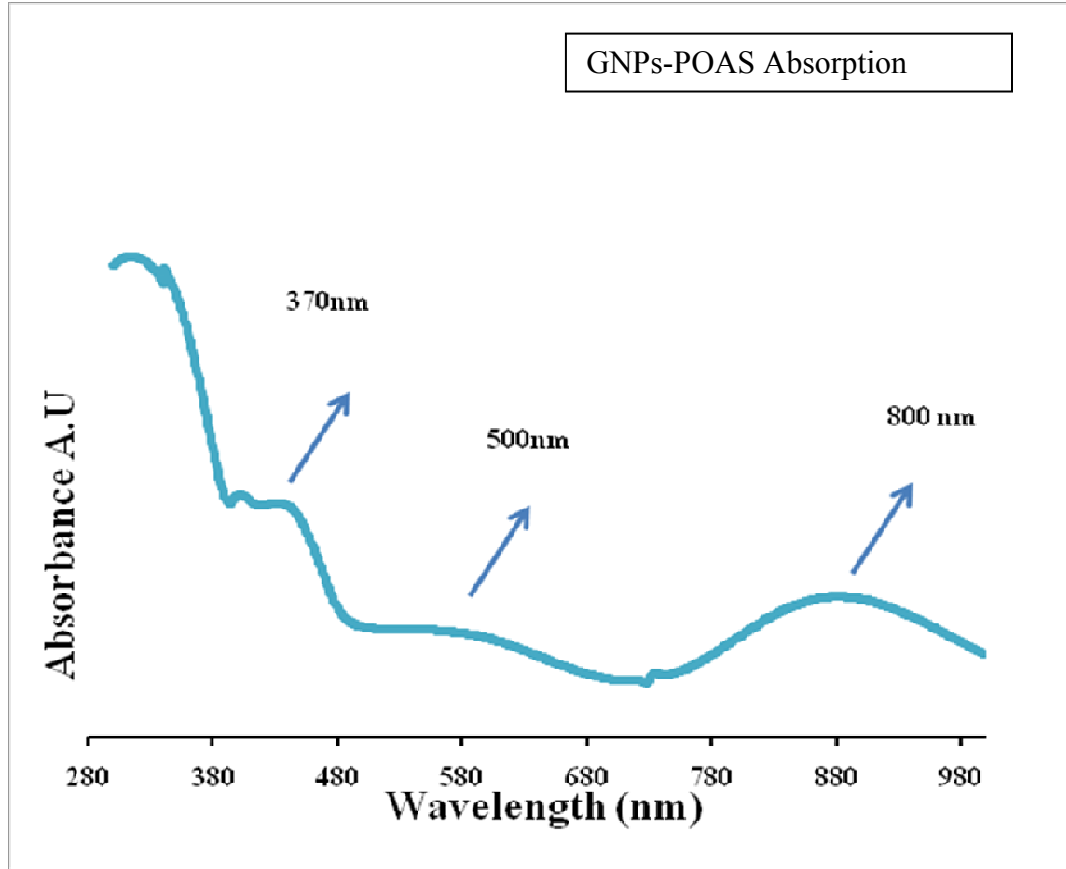


Figure 3.21 UV-vis Spectra of Composites POAS- GNPs

TEM images of the POAS and the composites of GNPs-POAS are shown in the figure 3.22 (a) and 3.22 (b). The TEM image of composites shows that the gold nanoparticles are well dispersed in the polymer.

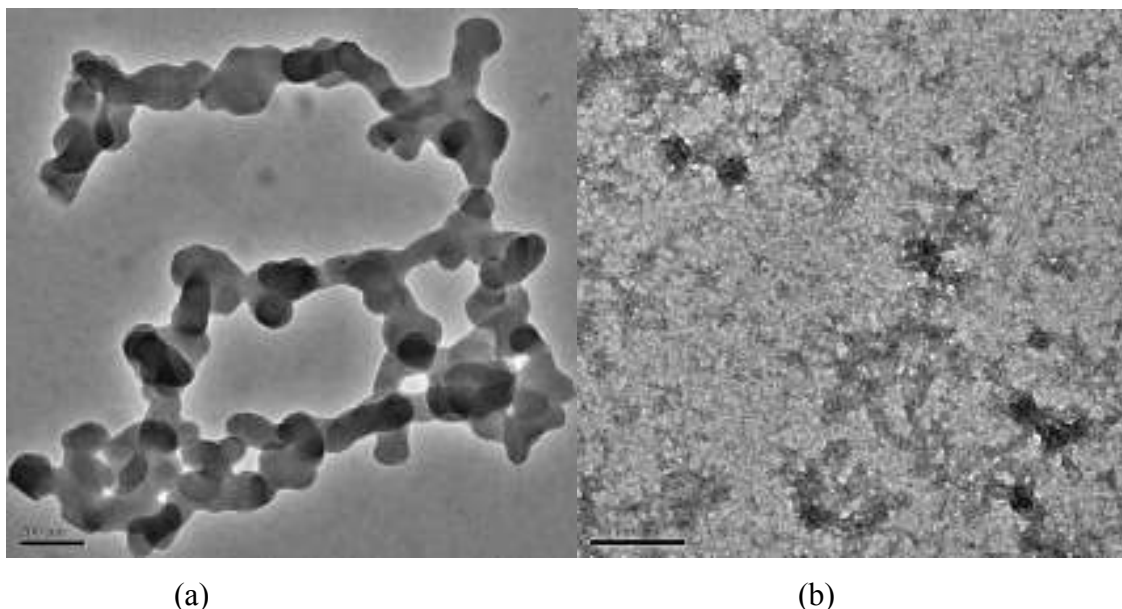


Figure 3.22 TEM Images, (a) POAS, (b) POAS-GNPs

The composite films made on silicon substrate were studied by Fourier Transform Infrared (FTIR) spectrophotometer. The IR spectra of POAS and GNPs were shown in figure 3.23. The gold nanoparticles exhibited a distinct peak at 1675 cm^{-1} . Moreover, the other peaks assigned for both POAS and gold-POAS composite are as follows. The peak observed in the POAS and GNPS-POAS (Stretch. quinoid ring) $\text{C}=\text{C}$ (1578 cm^{-1}), $\text{C}=\text{C}$ stretch, benzenoid ring ($1461, 1412\text{ cm}^{-1}$ in GNPs -POAS) and $\text{C}-\text{N}$ stretch (1343 cm^{-1}), 1337 cm^{-1} $\text{N}=\text{Q}=\text{N}$ (Q= quinoid ring) 1198 cm^{-1} $\text{C}-\text{H}$ stretching vibration, 1278 cm^{-1} . Furthermore, the FTIR analysis indicated that the composites of gold-POAS exhibited a better peak intensity.

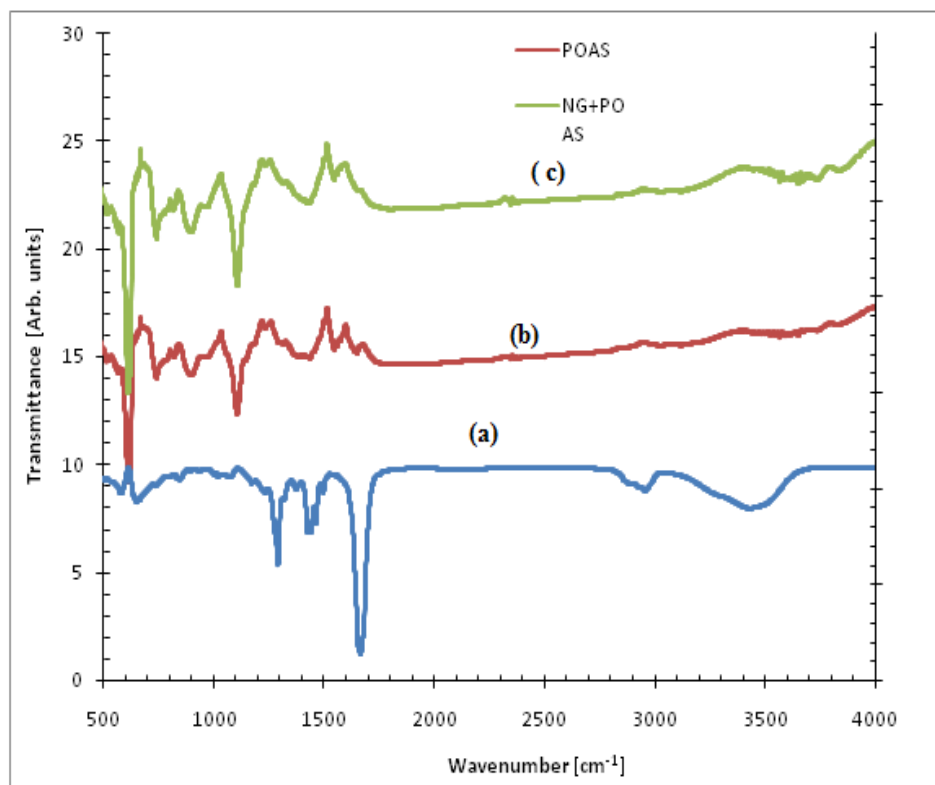


Figure 3.23 FTIR of (a) GNPs, (b) POAS, (c) POAS-GNPs

3.4 Electrochemical Characterization of GNPs-POAS

The electrochemical kinetics of composites of POAS and GNPs-POAS observed in 0.1M HCl were shown in figure 3.24 and 3.25 respectively. Cyclic voltammetry was performed in an electrochemical cell containing a three electrode set-up. Gold nanoparticles were immobilized on to the glassy carbon electrode and employed as the working electrode; platinum wire was utilized as the auxiliary electrode and Ag/AgCl as reference electrode. All the cyclic voltametric experiments were performed in 0.1M HCl at different scan rate (100 mVs^{-1} , 50 mVs^{-1} , 20 mVs^{-1} , 1 mVs^{-1}). Figure 3.24, represents the cyclic voltammograms of POAS in 0.1M HCl at different scan rates.

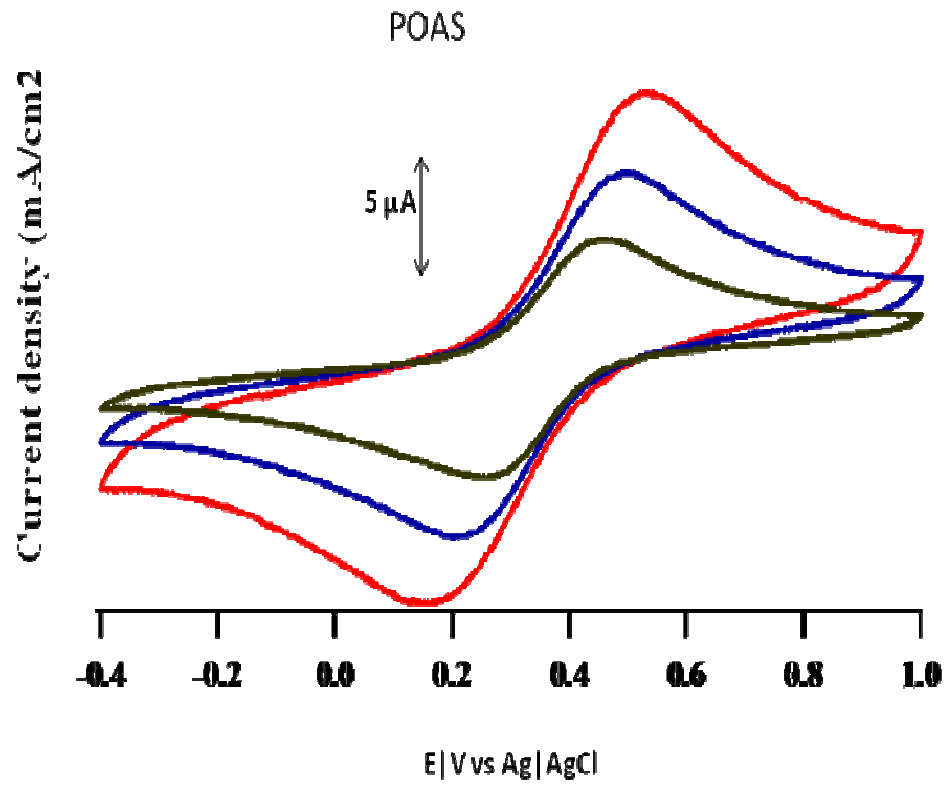


Figure 3.24 CV of POAS in Three Electrode System in 0.1M HCL

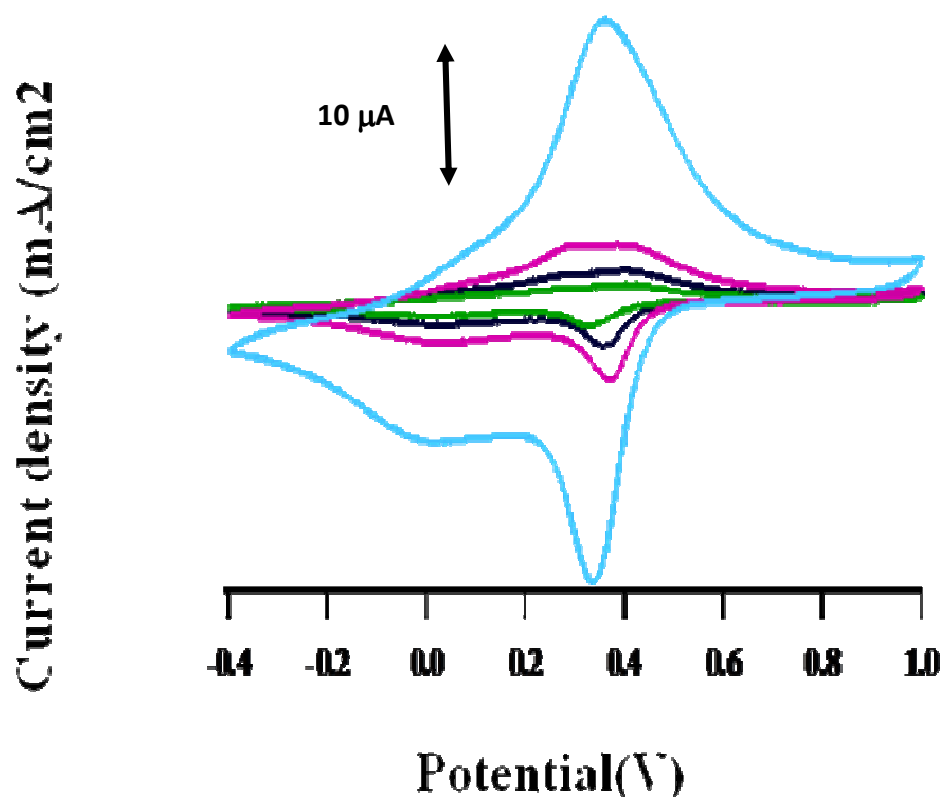


Figure 3.25 CV of POAS -GNPs in Three Electrode System in 0.1M HCL

On the other hand, the voltammograms of GNPs-POAS composites exhibited a pair of redox waves at 0.4V and 0.36V. However, the peaks are not well-defined. Of these two peaks the one at 0.18V was identical as that of polyaniline and the peak present at 0.4V corresponds to the oxidized form of POAS. In other words, the peak at 0.4V corresponds to the oxidized state whereas the peak at 0.36 V corresponds to the reduced state of NGs-POAS system. Interestingly, the peak at 0.4V, which is due to quinoid structure in NG-POAS, has a higher current than POAS as shown in Figure 3.25. Furthermore, Figure 3.25 indicates the characteristic peak of polyaniline systems of the polymer which was not observed in the case of polymer alone as shown by figure 3.24 thereby demonstrating

that the presence of Gold nanoparticles were not only useful for the redox reaction but also provide excellent probe for the polymer composite synthesis.

Chapter 4: Applications of GNPs

4.1 Introduction

In this chapter, we focused on the application of the chemically synthesized gold nanoparticles. The non-toxic nature of GNPs makes them a potential candidate for all the biological studies including the detection of biomolecules and in cancer therapy [36-38]. The inhibition of Respiratory Syncial Virus (RSV) by GNPs was described in detail in this chapter. RSV is the main cause of the pneumonia in children and may cause respiratory disorders [39-40] Studies on the interaction of gold nanoparticle with the protein Bovine Serum Albumin (BSA) were also described. Further, we have also described about the electrochemical detection of dopamine, uric acid and ascorbic acid using gold nanoparticle modified glassy carbon electrode. Finally, the applications of gold nanoparticles as catalytic activator for gas sensing have been discussed.

4.2 RSV Inhibition by GNPs

4.2.1 Cells and Virus

HEp-2 (Human body Type-2 epithelial cells) cells were purchased from American Type Culture Collection (ATCC, Manassas, VA; CCL-23) and were propagated by using Minimum Essential Medium (MEM) supplemented with 10% Fetal Bovine Serum (FBS),

2 mM L-Glutamine, 75 U/ml Penicillin, 100 mg/ml Kanamycin and 75 mg/ml Streptomycin. Human RSV Long strain was purchased from ATCC (VR# 26). Virulent RSV stocks were prepared and propagated in HEp-2 cells. RSV with multiplicity of infection of 4:1 was added to the flask and virus adsorption was carried out for 1h at 37°C in a humidified atmosphere with 5% CO₂. MEM supplemented with 2% FBS and 2 mM L-Glutamine was added to the flask and infection of cells was observed for 3 days. RSV infected cells were harvested and cell suspension was subjected to 2 freeze-thaw cycles at -80°C followed by centrifugation at 3,000 rpm at 4°C to remove the cellular debris. The viral stocks were aliquoted and stored at -80°C on liquid nitrogen until further use. Viral titer of the prepared stock was determined by plaque assay and had a titer of 10⁵ p.f.u / ml [39-40].

4.2.2 Preparation of GNPs and RSV Mixture

The gold nanoparticles (50µL/µL) were mixed with 20µL RSV containing 100 PFU, and incubated for 40 minutes at room temperature.

4.2.3 RSV Inhibition Experiment

RSV inhibition experiment was carried out by employing different concentrations of GNPs samples for RSV inhibition studies. The GNPs were mixed with 20mL of RSV containing 100 PFU and incubated for 30 minutes at room temperature. The GNPs-RSV complex was then added to 60–70% confluent HEp-2 cells in 8-chamber slides to observe the inhibition of RSV infection. HEp-2 cells infected with RSV without GNPs were used

as a positive control. The inhibition of RSV infection by each GNP sample was analyzed visually using an inverted light microscope as well as by indirect immunofluorescence using an Olympus IX51 immunofluorescence microscope. For indirect immunofluorescence, HEp-2 cells were grown in 8 chambered slides (BD Biosciences) for 24 h to 60% confluency. The cells were washed with phosphate buffered saline (PBS) and cured using 10% trichloroacetic acid for 15 min. The cells were then successively washed in 70%, 90%, and 100% ethanol for 5 min (in either case). Next, the cells were washed using PBS and incubated in blocking buffer (3% dry milk in PBS) for 30 min and washed thrice with PBS. The cured cells were incubated for 1h at room temperature with monoclonal mouse antibody to RSV F (Biodesign International) in antibody buffer (2% dry milk in PBS). The cells were washed three times for 5 min in PBS and then incubated for 1 h at room temperature with FITC-conjugated goat anti-mouse IgG (H+L) secondary antibody (Southern Biotechnology) in antibody buffer. Non-specific binding will be eliminated by washing the cell thrice in PBS and the cells were visualized using a fluorescent microscope [39-40]. The schematic of RSV inhibition experiment is represented in figure 4.1.

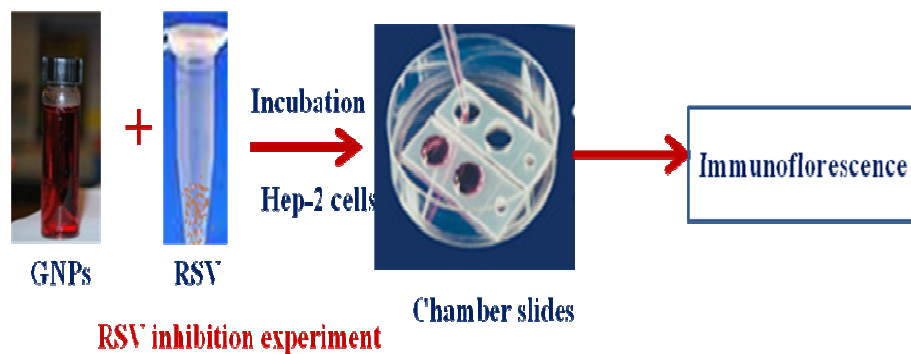


Figure 4.1 Schematic of RSV Inhibition Experiment

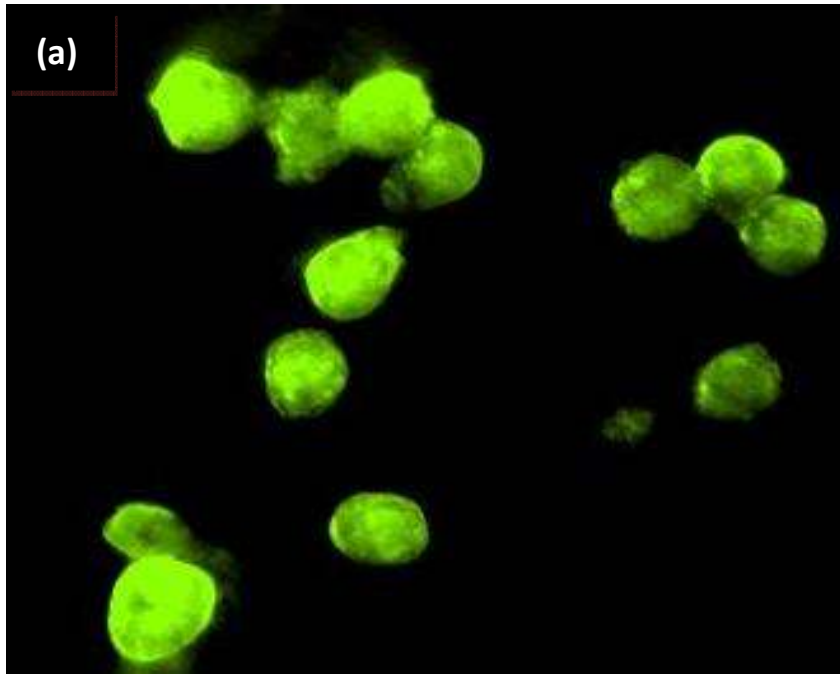


Figure 4.2 RSV Inhibition by Immunofluorescence Cells Infected with RSV

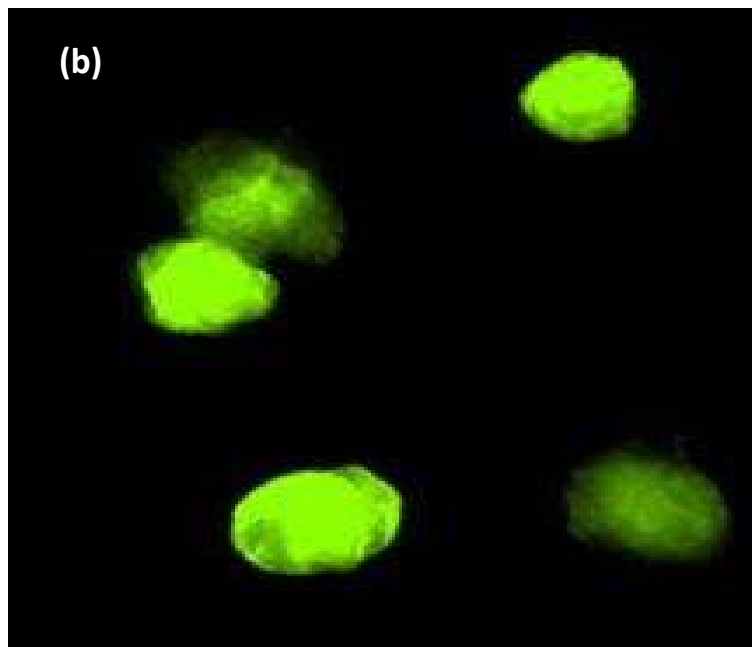


Figure 4.3 Cells Infected with RSV Mixed GNPs (5µl/ml)

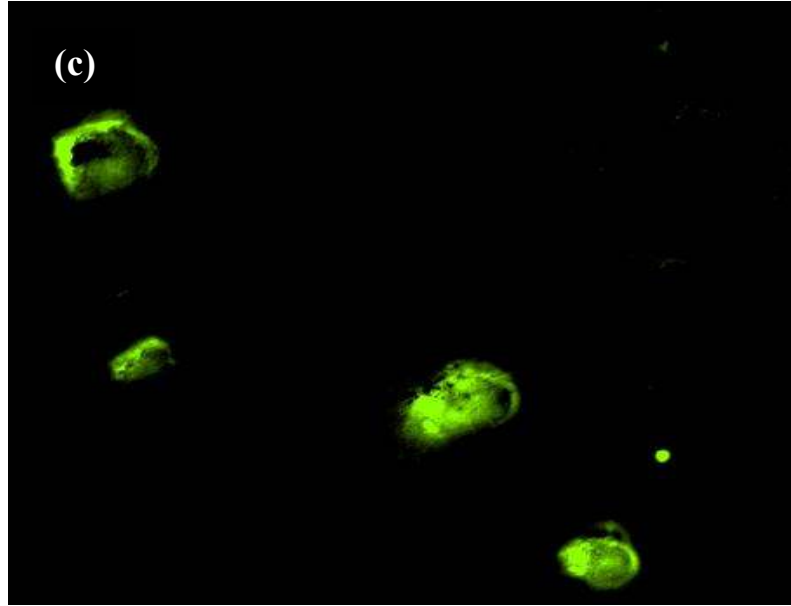


Figure 4.4 Cells Infected with RSV Mixed with GNP (50 μ l/ml)

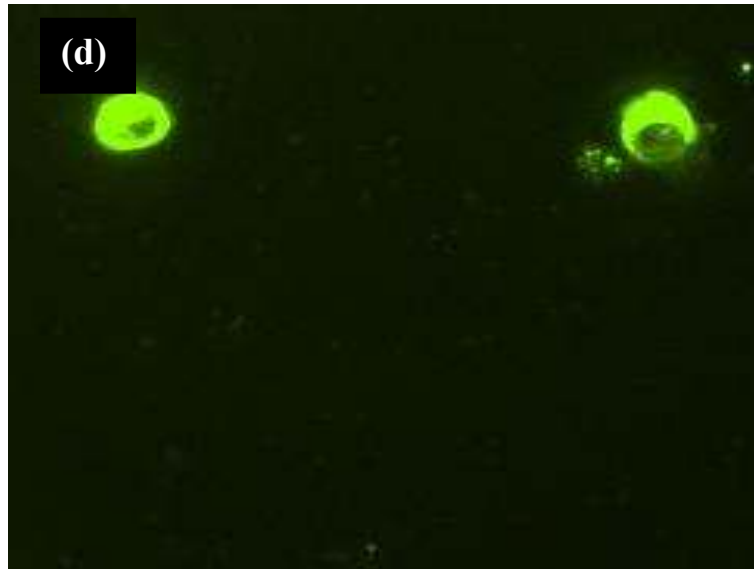


Figure 4.5 Cells Infected with RSV Mixed with GNP (100 μ l/ml)



Figure 4.6 Cells Infected with RSV Mixed with GNPs (200 μ l/ml)

GNPs were mixed with 100 PFU of RSV and added to the cells to determine the inhibition of infection. Reduction in cytopathic effects (syncytia) in HEp-2 cells was observed to determine the extent of RSV infection. Cell infection was monitored by immunofluorescence. Cells infected with RSV mixed with GNPs clearly showed a significant reduction in RSV infection compared to the cells infected with RSV alone. The results of the present study indicated that GNPs (10 nm) can inhibit RSV infection and in future it can be employed for the therapeutic purposes.

4.3 Biosensing Applications of the GNPs

Gold nanoparticles synthesized by the chemical methods have been utilized for the sensing application of neurotransmitters such as dopamine and the ascorbic acid

4.3.1 Detection of Neurotransmitters such as Dopamine, Ascorbic Acid

For many years, the study of brain and its associated processes have been an area of research to scientists with work focusing on issues ranging from the whole brain to single cell. Brain is one of the most complex biological matrices and is composed of approximately 100 billion nerve cells called neurons. Dopamine is an endogenous chemical compound that was discovered to be a neurotransmitter by Arvid Carlsson in the 1950s. Neurotransmitters are chemicals that facilitate the transport of the information between the neurons across the gap. Dopamine participates in the important brain functions and acts as a neurotransmitter and neurohormone, which inhibit the secretion of prolactin from the pituitary gland. Dopamine produces an effect on the sympathetic nervous system when used as a medication. Broadly, neurotransmitters were classified as indolamine, catecholamine, peptides, epinephrine, norepinephrine, amino acids, and acetylcholine. The structure of dopamine and ascorbic acid is shown in figure 4.7.

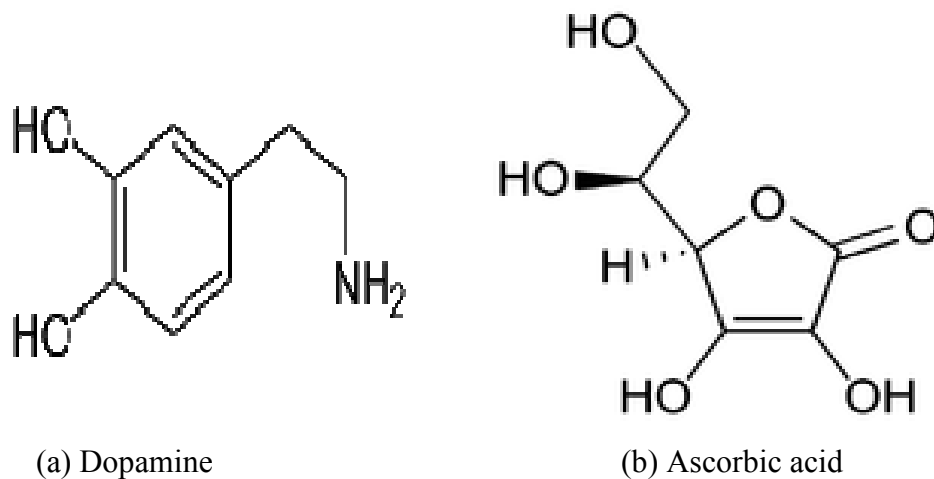


Figure 4.7 Structures of Dopamine and Ascorbic Acid

4.3.1.1 Importance of Monitoring Neurotransmitters

Monitoring various neurotransmitters is vital to understand the mechanism and pathways that leads to various behavioral changes and disorder. The neurotransmitters such as dopamine; ascorbic acid plays an important role in the regulation of motor function and associated with the mood swing and emotions. It is important to understand the mechanisms and kinetics of neurotransmitters such as dopamine. The low concentration of dopamine leads to Parkinson's disease, whereas the higher concentration causes Schizophrenia. Neurotransmitters including dopamine, ascorbic acid, uric acid, epinephrine and norepinephrine can be very easily oxidized electrochemically by applying a suitable potential. Based on this technique, in this work we employ glassy carbon electrode modified with gold nanoparticle as an electrode material to electrochemically detect the neurotransmitters [41-44]. Initially, glassy carbon electrodes were modified with gold nanoparticles and employed for the analysis. The modification of glassy carbon electrodes was performed as follows: The gold nanoparticles were synthesized chemically as described before by the citrate reduction method. 2 μ L of the GNP solution was casted to the glassy carbon electrode surface and dried at room temperature. This resulted in a uniform thin layer of GNP's on the electrode surface. In order to characterize the electrochemical redox behavior as well as the charge transfer properties of the GNPs, initially we employed different charged redox probes namely hexamine ruthenium (III) chloride and potassium ferricyanide. Cyclic voltammetry of these GNP's were performed initially in 1.0 mM $[\text{Ru}(\text{NH}_3)_6]^{3+/2+}$, a positively charged redox probe. Results indicated a well reversible redox peaks and confirming a one

electron transfer at the electrode surface. Following this, we have then performed the cyclic voltammetry of GNP's in 1.0 mM $[\text{Fe}(\text{CN})_6]^{3-/4-}$, a negatively charged redox probe. From these results, it is evident that GNP's are redox active irrespective of various charges present on the redox analyte, thereby, confirming its charge independent redox characteristics.

Further, we have evaluated the suitability of GNP's for the detection of certain important neurotransmitters such as dopamine (DA), ascorbic acid (AA). Additionally, we have also compared the performances of different sized GNP's (10 nm and 20 nm). Cyclic voltammograms of 20 nm GNP's in 1.0 mM DA, 1.0 mM AA are shown in Fig 4.8 and 4.10 respectively. On the other hand, upon comparing the signal to noise ratio and the limit of detection there is no marked difference in their response. Following this, we have also evaluated the effect of scan rate on the performance of GNP's (both 10 nm and 20 nm). In both cases, the plot of square root of scan rate against current density was found to be linear indicating a diffusion controlled process as shown in figure 4.9. We can conclude that GNP's are electroactive and can be employed for the detection of redox active biomolecules.

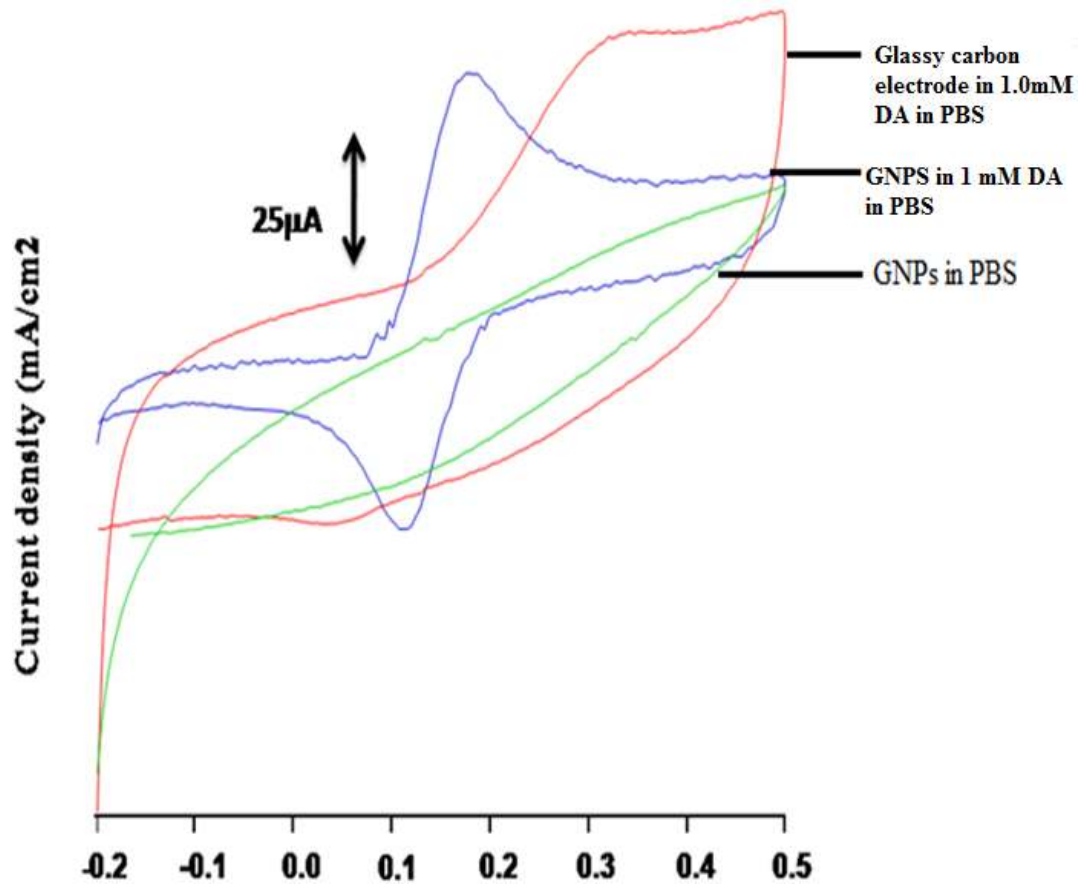


Figure 4.8 Cyclic Voltammogram of Dopamine in PBS

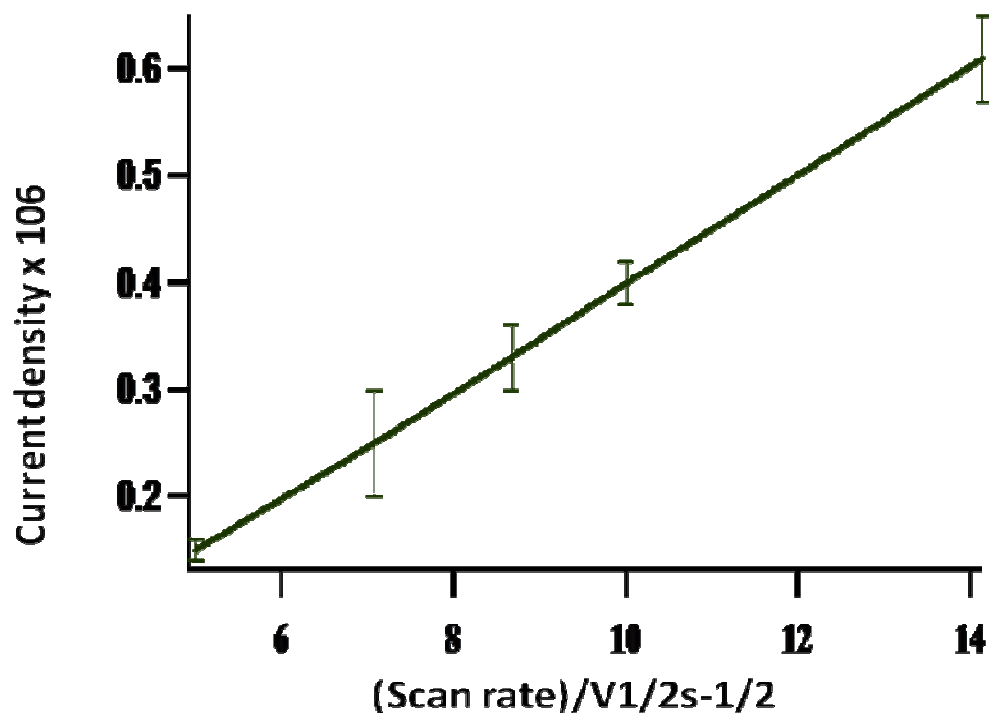


Figure 4.9 Scan Rate /Current Density Plot of Dopamine

Above mentioned analysis indicates that GNPs can expose itself completely to the analyte and provides efficient active sites essential for the redox reaction. In summary, we have studied the quasi-reversible and diffusion controlled electron transfer kinetics of dopamine, ascorbic acid at GNPs electrodes. The electrode response is stable over time with negligible electrode fouling.

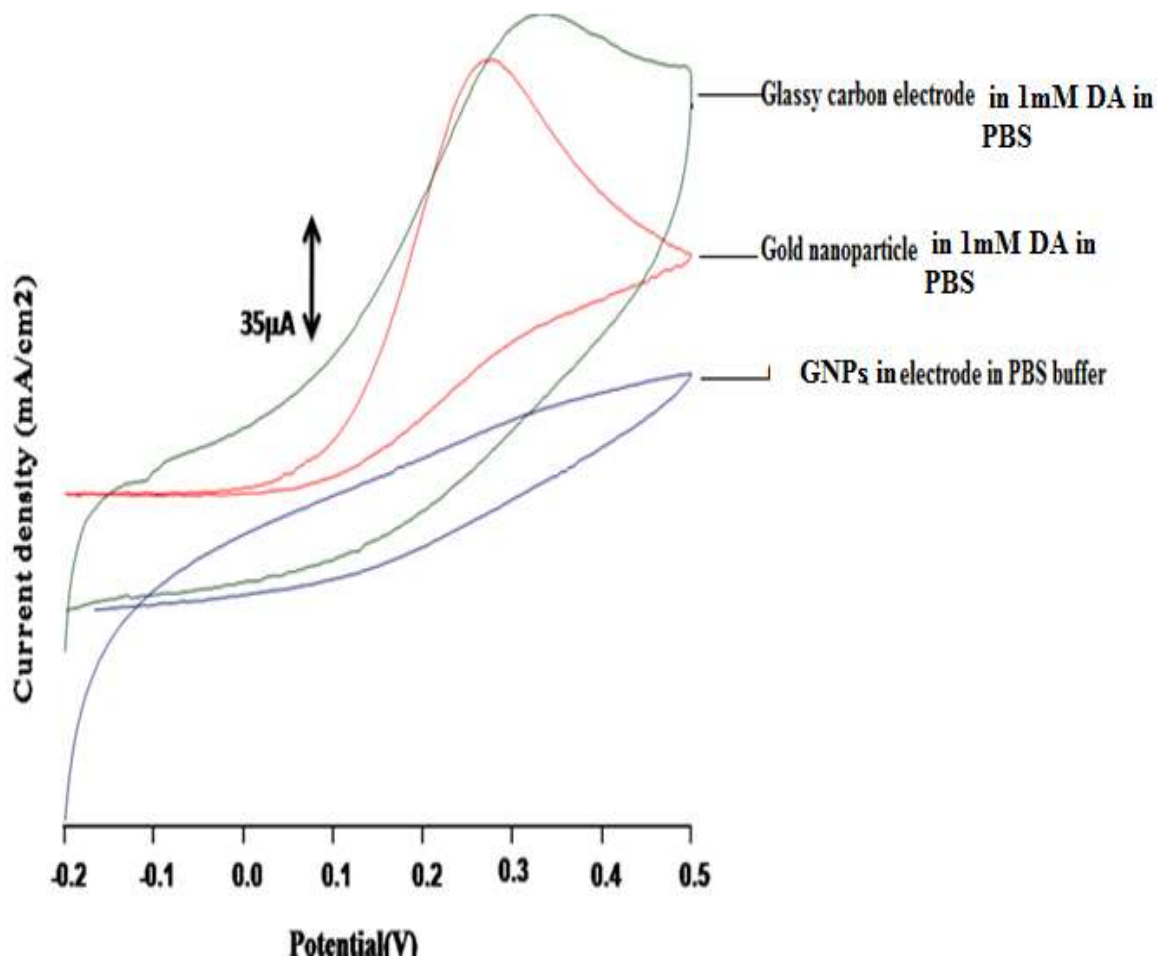


Figure 4.10 Cyclic Voltammogram of Ascorbic Acid in PBS

4.4. Analysis of GNPs-BSA Pair

In the literature there are several reports available that describes the interaction of GNPs and Bovine serum albumin [45-48]. The interaction was highly dependent on the size and concentration of GNPs. In general, the binding of GNPs with protein shows variation in the Surface Plasmon Resonance.

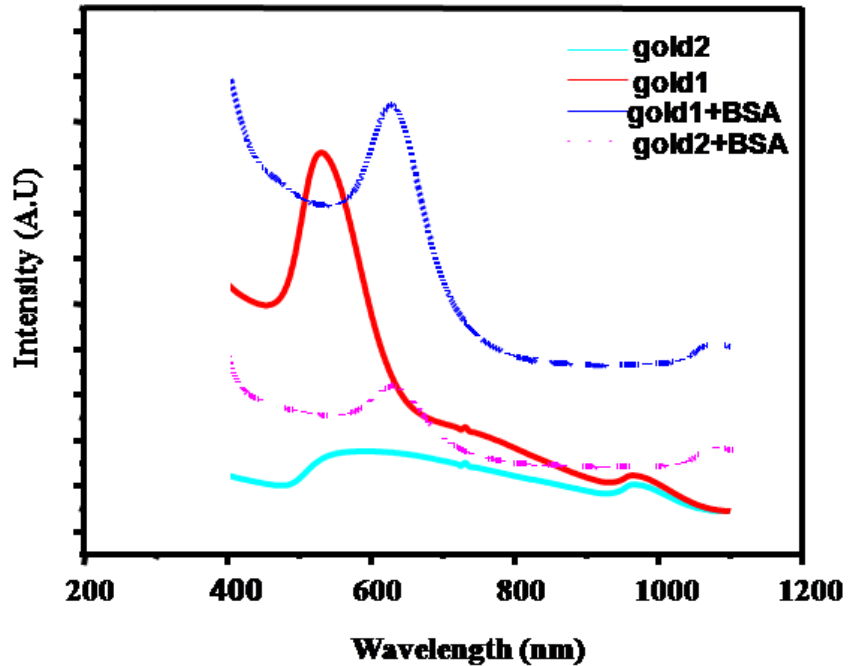


Figure 4.11 UV-vis Spectra of GNPs and GNPs-BSA (1~10 nm), (2~30nm)

Figure 4.11 shows the absorption spectra of GNPs and GNPs-Protein. As shown in the spectra it was obvious that the binding of protein to GNPs have altered the surface properties of the gold nanoparticles and caused the red shift in the absorption peak. Figure 4.12 and 4.13 represents the TEM images of GNPs and GNP-BSA particles. It was found that the GNPs with ~10 nm diameter showed dense aggregates due to the GNP-BSA interaction. However, GNPs with particle size > 20 nm does not exhibited much interaction with BSA. As the size of the nonmaterial decreases the efficient number of atoms increases in the surface which provide more efficient binding of the BSA onto NPs [45]. This observed phenomenon was further confirmed by the TEM measurements.

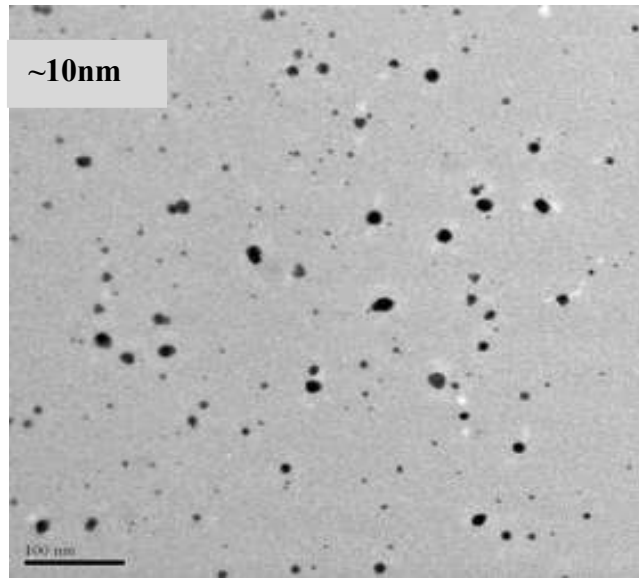


Figure 4.12 (a) TEM of GNPs (~10 nm)

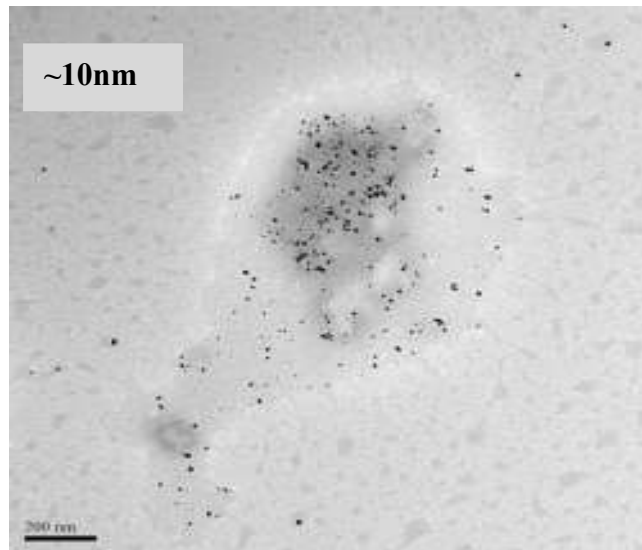


Figure 4.12 (b) TEM of GNPs-BSA Complex (GNPs~10 nm)

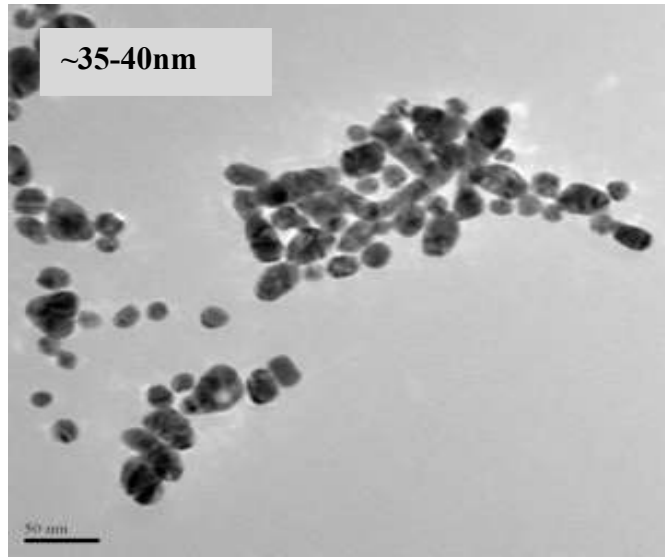


Figure 4.13 (a) TEM of GNPs (~35-40 nm)

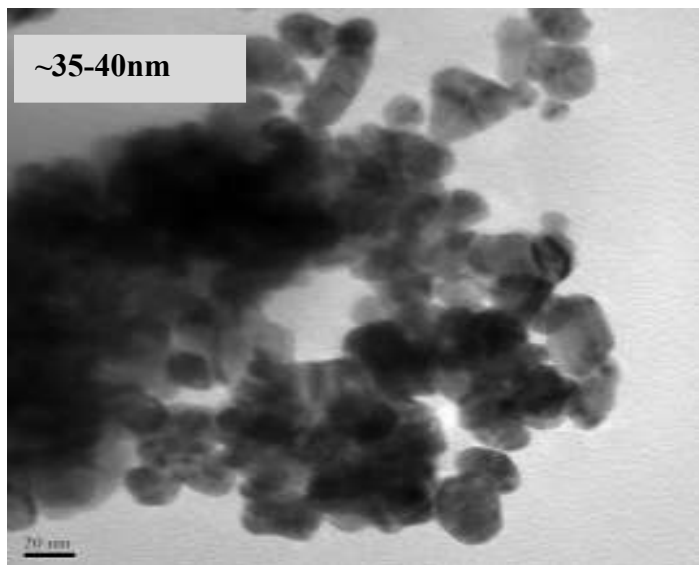


Figure 4.13 (b) TEM of GNPs-BSA (~35-40 nm)

Figure 4.12 Gold nanoparticles (a) GNPs 10nm, (b) 10 nm GNPs-BSA complex and 4-13 (a) and 4.13 (b) 30 nm GNPs and 30 nm GNPs-BSA respectively. This experiment shows that there is interaction of gold nanoparticles with the BSA. The interaction study was

done by UV-vis spectroscopy and TEM. The formations of aggregates of gold nanoparticles were observed by the TEM.

4.5 Catalytic Application of Chemically Synthesized GNPs

4.5.1 Au Decoration on ZnO Nanowires

In this work the chemically synthesized gold nanoparticles were utilized as catalyst for ZnO based gas sensors. TEM image in figure 4.14 (a) shows the size and shape of gold nanoparticles used for this purpose. ZnO nanowires were grown using vapor liquid solid growth method in our laboratory for other projects. Au nanoparticles were decorated on the body of the VLS grown ZnO nanowire using solution method to test their catalytic behavior. For this purpose, the ZnO nanowires were removed from the silicon substrate by sonification in methanol solution and a fixed quantity of Au nanoparticle solution was added to the ZnO nanowire solution. The resulting solution was mixed properly to allow the deposition of metal nanoparticle on the ZnO nanowires surface using slow stirring of the solution. Figure 4.14 (b) show the morphology of Au decorated ZnO nanowires. The white spots on the surface of ZnO nanowires are spherical gold nanoparticles in the size range 5-8 nm.

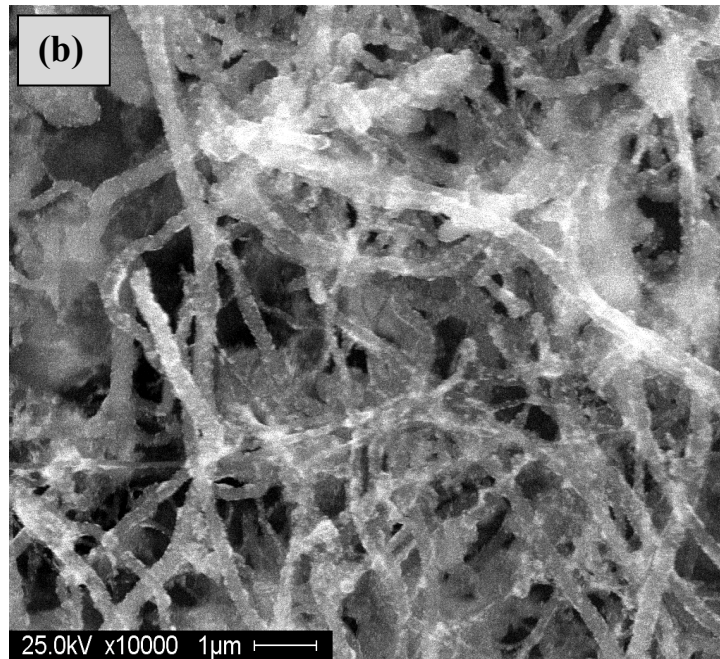
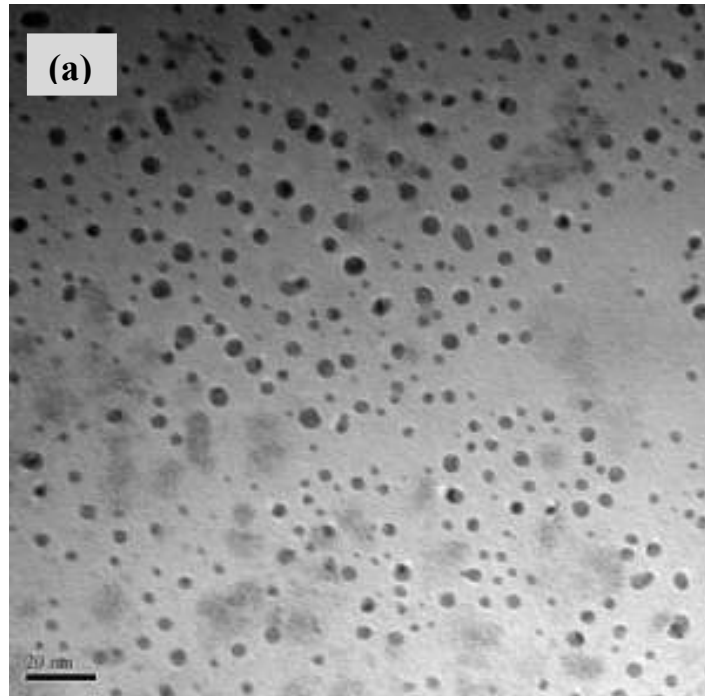


Figure 4.14 (a) TEM Image of GNPs, (b) SEM of ZnO Nanowire-GNPs

Au decorated ZnO nanowires were deposited by using drop cast method on top of the electrodes on the silicon substrate in order to develop the sensor.

The deposition of nanowires on substrate is followed by drying at 100°C in inert atmosphere for the duration of one hr. to get good electrical ohmic contact between the nanowire and electrodes. A proper deposition of the Au- ZnO nanowire on the electrodes shows a resistance value in the range of 4 k Ohm to 7 kOhm. Once the contacts are developed any two of the four electrodes were selected to measure the resistance of the sensor. The ZnO nanowire sensors were tested for gas sensing behavior by measuring the resistance in presence of compressed air and carbon monoxide using an electrometer (*Keithley 2400*) and a gas controller (*MKS 247*). Carbon monoxide sensing behavior of ZnO nanowire and Au decorated ZnO nanowires based sensors was studied in terms of variation of resistance with time for repeatedly switching of the gas from synthetic air (O₂) to various concentration of carbon monoxide (CO). The sensor signal is defined as percent change in resistance of the nanowire film upon CO exposure. If R_a is the resistance in air R_b is the resistance in presence of CO then the sensor signal is defined as $[(R_a - R_b)/R_a] \times 100\%$. Figure 4.15 shows the schematic of CO sensor assembly. There was no change in resistance (~1MOhm) for only ZnO nanowires at room temperatures for any concentration of CO between 100 to 1000 ppm [53].

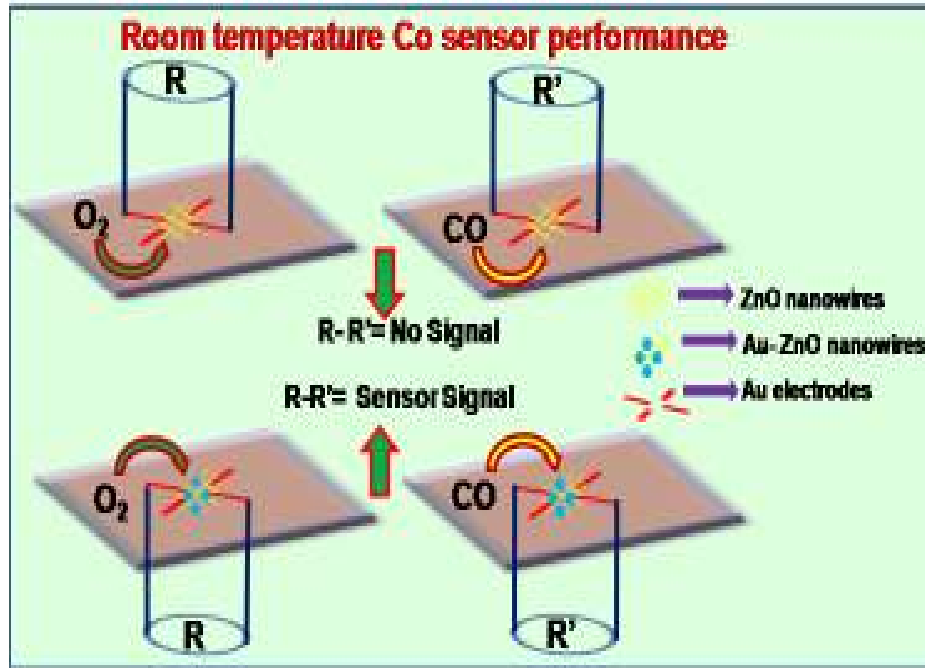


Figure 4.15 Assemblies of CO Sensors

However, for the Au decorated nanowires we have observed a decrease in resistance for all values of CO concentration at room temperature. Figure 4.16 shows the gas concentration vs. sensor signal $[(R_a - R_b)/R_a] \times 100\%$ data observed for the nanowire at room temperature while 8(b) show the sensor's performance at 200°C . On decorating the GNPs at the room temperature gas adsorption can be made possible due to the presence of Au on the surface. Adsorption of oxygen ions can occur on gold nanoparticle surface at room temperature due to the highly conductive nature and availability of free electron in gold. The conductive nanoparticle thereafter spills the gas over semiconductor surface via spillover effect [49-53].

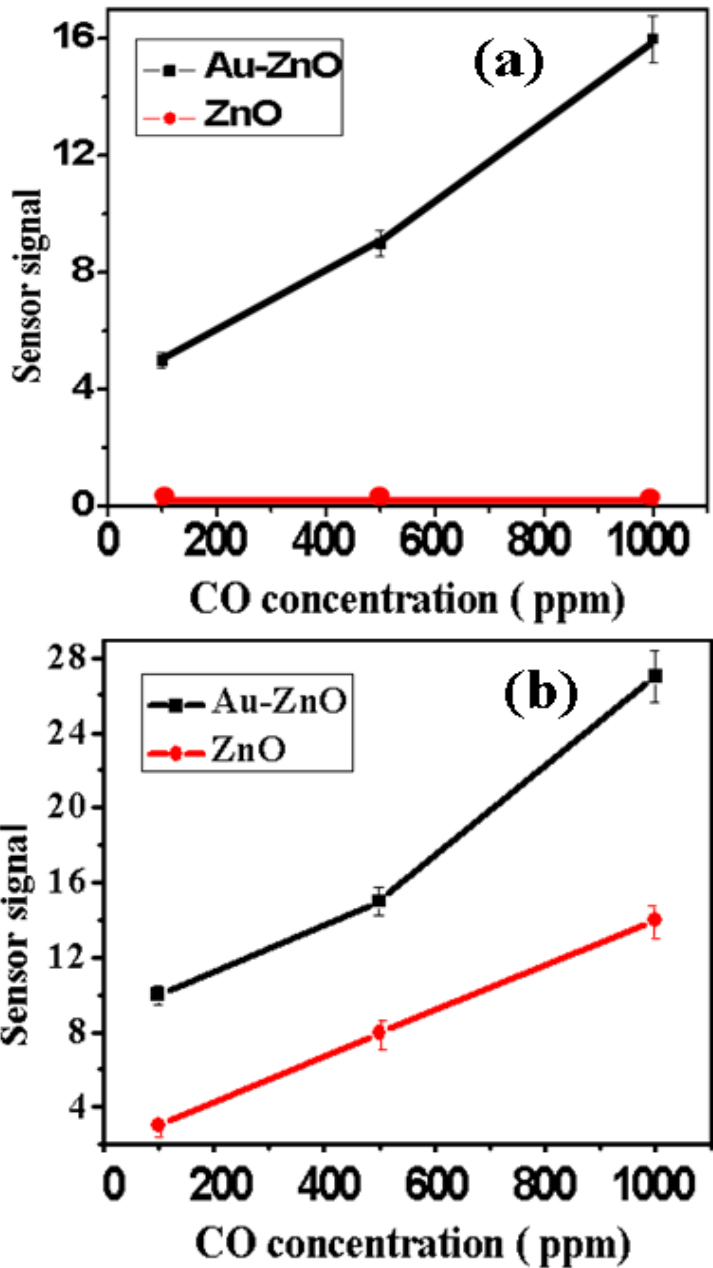


Figure 4.16 Variation of Gas Sensor Signal with CO Gas Concentration for ZnO and Au - ZnO Nanowires at (a) Room Temperature and (b) 200°C

The spillover effect via catalytic activation due to gold nanoparticle and chemical sensitization is observed to be responsible for room temperature CO sensing by Au decorated ZnO nanowires. Metal nanoparticles act as catalyst in chemical sensitization and improve the sensing characteristics. This study shows the applicability of gold nanoparticle as catalyst for gas sensor applications [53].

Chapter 5: Conclusions

The synthesis of gold nanoparticles with different shapes and sizes could be done by chemical method. The shape of the gold nanoparticles varied from nanospheres, nanocubes, triangles and nanooctagons. Control on the temperature, dilution and concentration of the reducing agent has been found to play an important role in defining the structure of gold nanoparticles.

An attempt has been made to synthesize the composites of POAS-GNPs by the oxidative polymerization technique. The composites of GNPs-POAS were studied by UV-vis spectroscopy, FTIR and TEM techniques. It has been found that the properties of this new material formed by the gold nanoparticles and conductive polymer POAS shows remarkable difference than POAS alone.

The systematic electrochemical studies of the gold nanoparticles are carried out in different solutions of electrolyte. Gold nanoparticles are casted on the electrode surface in order to study biosensing applications. The glassy carbon electrode surface is modified with the gold nanoparticles with different sizes for the detection of dopamine and ascorbic acid. Gold nanoparticles immobilized on the surface of glassy carbon provides better template for the detection.

The studies of the interaction of the gold nanoparticles with Bovine serum albumin in aqueous is done by UV-vis spectroscopy, and TEM techniques. The interaction leads to

the red shift of the SPR band of the gold nanoparticles. Gold nanoparticles can also be utilized as a catalyst.

Chapter 6: Future Work

Future work can be done in the following areas. Further studies on this area will definitely enhance the utilization of gold nanoparticles for the wide range of research studies.

(1) Gold nanorods and functionalized biocompatible gold nanoparticles are emerging as a promising tool for cancer diagnostic applications and medicine. So the future work can be done on their synthesis and fabrications to explore their other applications.

(2) The gold nanorods can also be utilized as biosensor applications. Biosensors are very active and interesting field of research. Metal nanoparticles can be synthesized and fabricated for the utilization of as template to study the various biological objects like protein, DNA and Nucleic acid.

References

1. V. Halte, J. Guille, J.C. Merle, I. Perakis, J.Y. Bigot, *Physical Review.B* 60, 11738 (1999)
2. P.A. Hervieux, A. Benabbas, V. Halte, J.Y. Bigot, *European Physical Journal D* 24, 185 (2003)
3. Kawabata, R. Kubo. *Journal of the Physical Society of Japan.* 21, 1765-1772 (1966)
4. G. Weick, G.L. Ingold, R. A. Jalabert, D. Weinmann, *Physical Review B.* 74, 165421 (2006).
5. Y. Bigot, V. Halte, J.C. Merle, A. Daunois, *Chemical Physics.* 251, 181-203 (2000)
6. T. V. Shabazyan, I. E. Perakis, J.Y. Bigot, *Physical Review Letters.* 81, 3120 (1998)
7. C. Voisin, D. Christofilos, N. Del Fatti, F. Vallée, B. Prével, E. Cottancin, J. Lermé, M. Pellarin M. Broyer. *Physical Review Letter.* 85, 2200 (2000)
8. <http://www-ipcms.u-strasbg.fr/spip.php?article1020&lang=fr>
9. <http://www.webexhibits.org/causesofcolor/9.html>
10. B. Valter, M.K.Ram, C.Nicolini, *Langmuir.* 18 (5), 1535–1541 (2002)
11. M. K. Ram, S. Carrere, S.Paddeu, E.Maccioni, C. Nicolini, *Langmuir.* 13 (10) 2760–2765 (1997).
12. B.Valter, S. Carrara, M.K.Ram, C. Nicolini, *Langmuir.* 20 (3), 969–973 (2004)
13. S. Paddeu, M.K.Ram, S. Carrara, C. Nicolini, *Nanotechnology.* 9, 3 (1998)
14. A.C. Balazs, T.Emrick, T.P. Russell, *Science.* 314 (5802), 1107 – 1110 (2006)

15. J.Y.Song, H.K.Jang, B. S.Kim, *Process Biochemistry*. 44, (10), 1133-1138 (2009)
16. J. Zhang, H. Liu, Z. Wang, N. Ming, *Advanced Functional Materials*. 17, 16, 3295–330 (2007)
17. J. Hu, Z.Wang, J. Li. *Sensors*. 7, 3299-3311 (2007)
18. J.E. Park, M.Atobe, T. Fuchigami. *Ultrasonics Sonochemistry*. 13, (3), 237-241 (2006)
19. X. Zhou, J.M. E. Khoury, L.Qu, L.Dai, Q. Li, *Journal of Colloid and Interface Science*. 308, (2), 381-384 (2007)
20. W. Wang, Q.Chen, C. Jiang, D. Yang, X. Liu, S. Xu, *Colloids and Surfaces A Physicochemical and Engineering Aspects*. 301, (5), 73-7 (2007)
21. J. Kasthuri, S. Veerapandian, N. Rajendiran, *Colloids and Surfaces: Biointerfaces*.68, (1), 55-60 (2009)
22. D. Philip, *Spectrochimica Acta Part A: Molecular and Bimolecular Spectroscopy*. 73, 4, 650-653 (2009)
23. J. Zhou, J.Ralston, R.Sedev, D.A. Beattie,*Journal of Colloid and Interface Science*. 331, 2, 251-262 (2009)
24. M. Nakamoto, Y.Kashiwagi, M. Yamamoto, *Inorganica Chimical Acta*.358, (14), 4229-4236 (2005)
25. N. Saito, J.Hieda, O. Takai, *Thin Solid Films*. 518, (3), 912-917 (2009)
26. Z. Ma, H.Han, *Colloids and Surfaces A: Physicochemical and Engineering Aspects*, 317, 1-3, 229-233 (2008)
27. P.Ravindra, *Materials Science and Engineering: B*. 163, (2), 93-98 (2009)
28. J. Jung, K. Na, J. Lee, K.-Woo Kim, J. Hyun. *Analytica Chimical Acta*, 651,(1), 91-97 (2009)
29. <http://www.unl.edu/ncmn/cfem/microscopy/TEM.shtml>

30. D. Kitenge, Master Thesis, University of South Florida, Tampa Florida, 2009
31. <http://nano.tm.agilent.com/blog/page/3/?s>
32. <http://www.ntmdt.com/spm-basics/view/probe-sample-interaction-potential>
33. <http://www.csun.edu/~jeloranta/CHEM352L/experiment3.pdf>
34. H.Yuan, W.Ma, C.Chen, J.Zhao, J.liu, H.Zhu, X. Gao, Chemistry of materials, 19 (7), 1592 –1600 (2007)
35. A. Sugunan, C.Thanachayanont, J. Dutta, P. Juilland, J.G. Hilborn, Proceedings of the International Conference on Smart/Intelligent Materials, Smart Material,(ISBN 974-656-288-8) 191-193 (2004)
36. C.R.Patra, R. Bhattacharya, D.Mukhopadhyay, P.Mukherjee, Advanced Drug Delivery Reviews. 62, (3), 346-361 (2010)
37. X. Huang, M. A. E. Sayed, Journal of Advanced Research. 1, (1), 13-28 (2010)
38. R. Bhattacharya, C. R. Patra, A. Earl, S.Wang, A. Katarya, L. Lu, J. N. Kizhakkedathu, M. J. Yaszemski, P.R. Greipp, D. Mukhopadhyay, P. Mukherjee Nanomedicine: Nanotechnology, Biology and Medicine. 3, (3), 224-238 (2007)
39. K. Vig, S. Byoglu, V. Rangari, M. Miller, S. Pillai, S. R. Singh, Biophysical Journal. 655a (2010).
40. S. Boyoglu, K. Vi, A. Pfenndt, S.Pillai, G. A Willing, S. R. Singh. Biophysical Journal. 98 3, 192a-192a (2010).
41. M. Pumera, S. Sánchez, I. Ichinose, Jie, Sensors and Actuators B: Chemical. 123, 2, 1195-1205(2007)
42. L. Zhang, X. Jiang. Journal of Electroanalytical Chemistry. 583, (2), 292-299 (2005)
43. M. T. Castañeda, S. Alegret, A. Merkoci, Electroanalysis. 19 (7-8), 743 – 753 (2007)
44. G. K. Vertelov, A. Yu. Olenin, V. Lisichkin, Journal of Analytical Chemistry. 62, 9903–915 (2007).

45. S. Pramanik, P. Banerjee, A. Sarkar, S.C. Bhattacharya, Journal of Luminescence. 128, 1969-1974 (2008).
46. M. Iosin, F. Toderas, P.L. Baldeck, S. Astilean, Journal of Molecular Structure. 924-926, 196-200 (2009)
47. S.Chah, M.R. Hammond, R. N. Zare, Chemistry & Biology. 12, (3), 323-328 (2005)
48. L.M. Ao, F. Gao, B.F.Pan, D.X. Cui, H.C. Gu, Chinese Journal of Chemistry 24, (2), 253 – 256 (2006)
49. R. K Joshi, F. E Kuris, Applied Physical Letters. 89, 153116 2007
50. A. Dieg'uez, A.Vila, A. Cabot, A. R. Romano, J. R.Morante, J. Kappler, N.Barsan, U. Weimar, W. Goepel, Sensors and. Actuators B., 68, (94) (2000)
51. S. Shukla, S. Seal, L. Ludwig, C. Parish, Sensors and Actuators, B. 97, (256) 2004
52. N. Yamazoe, Sensors and Actuators B. 5, (7) 1991
53. R. K. Joshi, Q. Hu, F. Alvi, N. Joshi, A. Kumar, Journal of Physical Chemistry C. 113 (36), 16199–16202 (2009)
54. <http://www.prenhall.com/settle/chapters/ch15.pdf>

About the Author

Nidhi Joshi has received her Bachelor of Science in 2002 and Master of Science in Chemistry with first rank from Kumaon University Almora in 2004. In January 2009, Nidhi was enrolled for the Master of Science in Material Science & Engineering program. Nidhi was a graduate research assistant for the Mechanical Engineering department University of South Florida. After completing this program she would like to do Ph. D. in nanomaterials technology.